

GROWTH OF GaN-BASED LED ON C-PLANE GaN SUBSTRATE

SIVANATHAN A/L PARIASAMY @ CHELLADURAI

**FACULTY OF SCIENCE
UNIVERSITY OF MALAYA
KUALA LUMPUR**

2018

**GROWTH OF GaN-BASED LED ON C-PLANE GaN
SUBSTRATE**

SIVANATHAN A/L PARIASAMY @ CHELLADURAI

**DISSERTATION SUBMITTED IN FULFILMENT OF THE
REQUIREMENTS FOR THE DEGREE OF MASTER**

**DEPARTMENT OF PHYSICS
FACULTY OF SCIENCE
UNIVERSITY OF MALAYA
KUALA LUMPUR**

2018

UNIVERSITI MALAYA

ORIGINAL LITERARY WORK DECLARATION

Name of Candidate: **SIVANATHAN A/L PARIASAMY**

Registration/Matrix No.: **SGR160037**

Name of Degree: **MASTER OF SCIENCE**

Title of Project Paper/Research Report/Dissertation/Thesis ("this Work"):

GROWTH OF GaN-BASED LED ON C-PLANE GaN SUBSTRATE

Field of Study: **EXPERIMENTAL PHYSICS**

I do solemnly and sincerely declare that:

- (1) I am the sole author/writer of this Work;
- (2) This work is original;
- (3) Any use of any work in which copyright exists was done by way of fair dealing and for permitted purposes and any excerpt or extract from, or reference to or reproduction of any copyright work has been disclosed expressly and sufficiently and the title of the Work and its authorship have been acknowledged in this Work;
- (4) I do not have any actual knowledge nor do I ought reasonably to know that the making of this work constitutes an infringement of any copyright work;
- (5) I hereby assign all and every rights in the copyright to this Work to the University of Malaya ("UM"), who henceforth shall be owner of the copyright in this Work and that any reproduction or use in any form or by any means whatsoever is prohibited without the written consent of UM having been first had and obtained;
- (6) I am fully aware that if in the course of making this Work I have infringed any copyright whether intentionally or otherwise, I may be subject to legal action or any other action as may be determined by UM.

Candidate's Signature

Date:

Subscribed and solemnly declared before,

Witness's Signature

Date:

Name: Dr. Ahmad Shuhiami bin Abu Bakar

Designation: Doctor and Supervisor

GROWTH OF GaN-BASED LED ON C-PLANE GaN SUBSTRATE

ABSTRACT

The InGaN/GaN multi-quantum wells, growth on bulk GaN substrate were studied for blue light emission via metal-organic chemical vapor deposition (MOCVD). The homo-epitaxy growth of GaN-on-GaN gives an unprecedented high performance with low defect density, high-quality crystal, simplified LED architectures (short process flow) and overall lower cost. The optimizations of InGaN/GaN MQWs on n-type GaN substrate for blue emission at 445-455 nm range were carried out. The high quality 6 pairs of multi-quantum wells with InGaN quantum wells and GaN quantum barriers were grown at different temperatures (650 °C to 780 °C). The lowest defect density demonstrated at $1.3 \times 10^7 \text{ cm}^{-2}$ on multi-quantum wells with quantum wells and quantum barrier temperature at 697 °C and 777 °C, respectively using atomic force microscopy. A full structured blue LEDs was successfully grown with peak wavelength emission at 449 nm, forward voltage at 4.5 V and the light output power at 2.0 mW at given current density at 20 mA/cm². A unique observation found there is heat interaction effect between the bulk GaN substrates and surrounded by the sapphire corral. The same multi-quantum wells growth conditions exhibited differently compared to that of a whole sapphire substrate (absence of GaN). The predicted surface temperature of bulk GaN substrate is 10 °C-15 °C of more than the corral sapphire. This observation may link to the thermal distribution difference of the growth surface corresponding to the different thermal conductivity ratio. The photoluminescence and computational techniques were used to understand in-depth of the heat interaction.

Keywords: Thermal conductivity, bulk GaN substrate, blue light emission, PL

PERTUMBUHAN LED BERASASKAN GaN PADA SATAH C SUBSTRAT GaN

ABSTRAK

Pertumbuhan perigi kuantum berbilang InGaN /GaN pada substrat GaN pukal telah dikaji untuk emisi cahaya biru menggunakan pemendapan wap kimia organik-logam (MOCVD). Pertumbuhan homo-epitaxy GaN pada GaN memberikan prestasi tinggi dengan ketumpatan kecacatan rendah, kristal berkualiti tinggi, seni bina LED yang lebih mudah (aliran proses pendek) dan keseluruhan kos yang rendah. Pengoptimuman InGaN /GaN MQWs pada GaN n-jenis untuk pelepasan cahaya biru pada jarak 445-455 nm telah dijalankan. 6 pasang berkualiti tinggi dengan perigi kuantum InGaN dan halangan kuantum GaN pertumbuhan dengan berlainan suhu (650 °C hingga 780 °C). Ketumpatan kecacatan terendah adalah $1.3 \times 10^7 \text{ cm}^{-2}$ pada perigi kuantum berbilang dengan perigi kuantum pada suhu 697 °C manakala halangan kuantum pada suhu 777 °C dengan menggunakan mikroskopi tenaga atom. LED biru berstruktur penuh berjaya ditumbuh dengan pelepasan panjang gelombang puncak pada 449 nm, voltan hadapan pada 4.5 V dan cahaya kuasa output pada 2.0 mW dengan kepadatan arus yang diberikan pada 20 mA/cm². Didapati terdapat kesan interaksi haba antara substrat GaN pukal dan dikelilingi oleh "sapphire". Keadaan pertumbuhan perigi kuantum yang sama akan tetapi menunjukkan perbezaan berbanding dengan substrat sapphire (ketiadaan GaN). Permukaan suhu substrat GaN pukal diramalkan adalah 10 °C -15 °C lebih dari "sapphire" Perbezaan taburan haba pada permukaan pertumbuhan disebabkan oleh nisbah kekonduksian terma yang berbeza. Fotoluminesen dan teknik pengiraan digunakan untuk memahami secara mendalam interaksi haba

Katakunci: Kekonduksian terma, pukal GaN substrat, emisi cahaya biru, PL.

ACKNOWLEDGEMENTS

This thesis would never have been written easily without the help and support of these people. Therefore, I would like to thank to them in this humble acknowledgement. First and foremost, my most sincere and profound appreciation goes to Prof. Datin Dr. Saadah Binti Abdul Rahman who allowed me to work under LDRMC group support. Subsequently to my supervisor Dr. Shuhaimi for his instrumental support in assisting me to complete this thesis. His valuable guidance, patience through my study. I am extremely grateful to Prof. Steven DenBaars, Prof. Shuji Nakamura and Prof. Jim Speck from UCSB for their valuable knowledge sharing through CREST collaboration. Thank you, my respected laboratory mates for helping to build the good rapport and conducive environment for carrying out research together. My heartfelt appreciation also goes to my family always for their moral support. My final acknowledgement goes out to the ONE who has no attribution. HE is eternal, higher consciousness and bliss state.

TABLE OF CONTENTS

ABSTRACT	iii
ABSTRAK	iv
ACKNOWLEDGEMENTS	v
TABLE OF CONTENTS	vi
LIST OF FIGURES	ix
LIST OF TABLES	xii
LIST OF SYMBOLS AND ABBREVIATIONS	xiii
LIST OF APPENDICES	xiv
CHAPTER 1: INTRODUCTION	1
1.1 Background	1
1.2 Objectives of the Present Investigation	3
1.3 Scope of the Thesis	4
CHAPTER 2: LITERATURE REVIEW	6
2.1 Introduction.....	6
2.2 Nitride-III group	6
2.2.1 Crystal structure and properties of III-V	7
2.2.2 Energy band.....	9
2.2.3 Polarization and Stack effect	11
2.3 Nucleation and growth	12
2.4 Defect related to GaN epitaxial.....	13
2.5 GaN-on-GaN LEDs performance	14
2.6 GaN epitaxial layer on polar <i>c</i> -plane bulk GaN vs sapphire.....	15
2.7 A brief history of GaN-based Blue LED research.....	16
CHAPTER 3: EXPERIMENTAL MATERIALS AND METHODOLOGY	19

3.1	Introduction.....	19
3.2	Overview of research work	20
3.3	Metal organic chemical vapor deposition, MOCVD	21
3.4	Material preparation and growth on <i>c</i> -plane bulk GaN substrates	23
3.4.1	Sample preparation.....	23
3.4.2	Growth condition.....	23
3.5	Characterization.....	24
3.5.1	Analyzing structural and optical properties.....	25
3.5.2	Electrical characterization	27
CHAPTER 4: RESULTS AND DISCUSSION: DEFECT ANALYSIS ON		
C-PLANE GaN.....		28
4.1	Introduction.....	28
4.2	Growth of Undoped and n-type GaN layer on bulk GaN substrates.....	28
4.3	Insertion n-type strained-layer superlattices, SLS layer.....	30
4.3.1	Without SLS	30
4.3.2	With SLS	32
4.4	GaN cap optimization for higher temperature barrier, HT-Barrier.....	34
4.5	Higher Temperature Barrier Growth, HT-Barrier.....	35
4.6	Summary	37
CHAPTER 5: RESULTS AND DISCUSSION: BASIC TARGET OF		
BLUE LED.....		38
5.1	Introduction.....	38
5.2	Performance Target for Epitaxial Growth	38
5.2.1	Data and analysis.....	39
5.3	Summary	49

CHAPTER 6: RESULTS AND DISCUSSION: DEMONSTRATION OF FIRST GaN-ON-GaN BLUE LED IN MALAYSIA	50
6.1 Introduction.....	50
6.2 First GaN-on-GaN Blue LED	50
6.3 Summary	53
CHAPTER 7: RESULTS AND DISCUSSION: NOVEL FINDINGS; EFFECT OF THERMAL INTERACTION BETWEEN BULK GAN SUBSTRATES AND CORRAL SAPPHIRE.....	54
7.1 Introduction.....	54
7.2 Observation	54
7.3 Analysis using simulation method by COMSOL.....	57
7.4 Summary	61
CHAPTER 8: CONCLUSION AND SUGGESTIONS	62
REFERENCES.....	64
LIST OF PUBLICATIONS AND PAPERS PRESENTED	70
APPENDICES	71

LIST OF FIGURES

Figure 2.1	: Bandgap energy vs lattice constant for typical semiconductors (Bayo, 2013).....	7
Figure 2.2	: GaN unit cell structure (Miguel et al., 2014)	8
Figure 2.3	: Crystal structure for GaN, with unit cell (blue dashed line), dipole moment (red arrow) and lattice parameters a and c denoted in red (Ren, 2016)	8
Figure 2.4	: Wurtzite structure, left: Miller indices for, right: Orientation of a-,m-, and r- (Imer et al., 2012)	9
Figure 2.5	: Left: Direct band gap, Right: Indirect band gap (Gupta et al., 2015)	10
Figure 2.6	: Band diagram of MQWs, GaN/InGaN/GaN (Ren, 2016)	10
Figure 2.7	: Influence of polarization induced electric field (Speck & Chichibu, 2009)	12
Figure 2.8	: Thermal and lattice mismatches in the growth of heteroepitaxy (Nakamura & Krames, 2013).....	15
Figure 2.9	: Comparison TEM images between GaN-on-GaN and GaN on Si	16
Figure 3.1	: Horizontal MOCVD reactor	21
Figure 3.2	: Horizontal three-layer laminar-Flow Channel (Matheson, 2015).....	22
Figure 3.3	: Bulk GaN substrates and sapphire corral arrangement on wafer carrier	23
Figure 3.4	: Left: Basic schematic of the GaN-on-GaN blue LEDs structure, Right: Blue light emission.....	24
Figure 4.1	: The first layer on bulk GaN substrates.....	28
Figure 4.2	: Sample G007-Undoped GaN, Left: Surface under image microscope under 200X, Middle: AFM scan image , and Right: FESEM scan image.....	29
Figure 4.3	: RMS of surface roughness, Left: Sample G074, Right: Sample G075	29
Figure 4.4	: Sample G043, Left: Structure without SLS, Right: Omega-2theta from XRD	30
Figure 4.5	: Sample G043, Left: AFM scan image on MQWs structure without SLS layer, Right: AFM depth profile	31

Figure 4.6	: Sample G043, Left: CL scan image of MQWs structure without SLS layer, Right: CL spectrum	32
Figure 4.7	: Sample G046, MQWs structure with SLS layer	32
Figure 4.8	: Sample G046, Left: AFM scan image AFM scan image on MQWs structure with SLS layer, Right: AFM depth profile	33
Figure 4.9	: Sample G046, Left: CL scan image AFM scan image of MQWs structure with SLS layer, Right: CL spectrum	33
Figure 4.10	: Details for MQWs.....	35
Figure 4.11	: Left: MOWs structure, Right: PL spectrum.....	35
Figure 4.12	: AFM image, Left: G054, Right: G055	36
Figure 5.1	: Left: Schematic of GaN-on-GaN LEDs structure , Right: Blue light emission.....	38
Figure 5.2	: Sample G060 ₃ , Left: SIMS stack series, Right: SIMS result	39
Figure 5.3	: SIMS results, Left: Samples G074, Right: Samples G075	40
Figure 5.4	: Left: Sample G007, Right: Sample G008	41
Figure 5.5	: Left: Sample G007, Right: Sample G008	41
Figure 5.6	: RMS of surface roughness on Uid-GaN, Sample G007 at 0.48 nm....	42
Figure 5.7	: [Si], Top: Sample G074, Bottom: Sample G075	43
Figure 5.8	: Surface roughness, Left: Sample G074, Right: Sample G075	46
Figure 5.9	: CL spectrum, Left: Sample G046, Right: Sample G073	47
Figure 5.10	: Light output power and voltage vs current	48
Figure 5.11	: EL wavelength spectrum.....	49
Figure 6.1	: Blue GaN-on-GaN LEDs partially grown in Malaysia and UCSB	50
Figure 6.2	: Blue GaN-on-GaN LEDs partially grown in Malaysia and UCSB: EL spectrum.....	51
Figure 6.3	: Blue GaN-on-GaN LEDs partially grown in Malaysia and UCSB, I-V curve	51
Figure 6.4	: Blue GaN-on-GaN LEDs fully grown in Malaysia for device no. G072 and G073.....	52

Figure 6.5	: EL spectrum for device no. G072 and G073 of blue GaN-on-GaN LEDs fully grown in Malaysia	53
Figure 7.1	: Sample A, B, and C's wavelength spectrum from PL	55
Figure 7.2	: Rapid thermal processing plan used in this model	58
Figure 7.3	: Wafer temperature profile of GaN-sapphire and sapphire from COSMOL simulation.....	59

University of Malaya

LIST OF TABLES

Table 1.1	: Targets of the 12 key parameters of GaN Epitaxial Growth.....	4
Table 4.1	: With and without SLS comparison	34
Table 4.2	: GaN cap optimization table.....	35
Table 4.3	: Comparison between LT (697 °C) and HT (777 °C) barrier condition	36
Table 5.1	: Growth rate of n-GaN	40
Table 5.2	: XRC-FWHM of the 002 and 102 plan and the screw N_{screw} and edge N_{edge} dislocation densities for G007 and G008	42
Table 5.3	: n-GaN Silicon concentration.....	44
Table 5.4	: n-GaN sheet resistivity and resistivity	45
Table 5.5	: MQW Blue light emission met the targeted range of 455 nm \pm 10 nm	46
Table 5.6	: SIMS result, refer to Figure 4.1 for G060 ₁ at 35 sccm and G060 ₂ at 20 sccm	47
Table 5.7	: L-I-V result.....	48
Table 6.1	: Blue GaN-on-GaN LEDs fully grown in Malaysia	52
Table 6.2	: Blue GaN-on-GaN LEDs fully grown in Malaysia for device no. G072 and G073	53
Table 7.1	: Sample A grown on whole sapphire, sample B and C on bulk GaN substrates with sapphire corral	55
Table 7.2	: Summary of previous research on growth with different substrates	56
Table 7.3	: GaN and sapphire constants	58
Table 7.4	: Maximum temperature difference in the wafer for different substrate types from the COSMOL simulation	60
Table 7.5	: Simulated temperature of MQW	60
Table 7.6	: Re-corrected MQW temperature.....	61

LIST OF SYMBOLS AND ABBREVIATIONS

MOCVD	:	metal-organic chemical-vapor deposition
MOMBE	:	metal-organic molecular-beam epitaxy
MOVPE	:	metal-organic vapor-phase epitaxy
MQW	:	multiquantum well
MBE	:	molecular-beam epitaxy
PL	:	photoluminescence
SIMS	:	secondary ion mass spectrometry
SLS	:	strain layer superlattice
TEGa	:	triethylgallium
TMGa	:	trimethylgallium
TMIn	:	trimethylindium

LIST OF APPENDICES

Appendix A: Recipe and growth condition of sample G043	71
Appendix B: Hall measurement.....	72

University of Malaya

CHAPTER 1: INTRODUCTION

1.1 Background

The great achievement of the 20th century in lighting field is bulbs and fluorescent lamps invention. In the 21st century, the tremendous achievement in solid-state physics has been light emitting diodes (LEDs). LEDs are smarter choice compared to conventional light sources such as light bulbs or fluorescent lamps. Technically, LEDs has high efficient and improved lifetime and even much brightness compared to conventional light sources. Research of LEDs conducted to obtain a high luminescence efficiency, quick response-to-time and longer lifetime. The efficacy of a lighting source is expressed in units of lumen per watt. The lumen is unit that measures the light power convoluted by the response of the human eye. As commercial users are yet to familiar with scientific term called lumens, this led manufacturers display strange energy-saving bulbs equations, such as $11.5\text{ W} = 75\text{ W}$, meaning: with 11.5 W of electrical power for LED bulbs gets same brightness for a traditional incandescent light bulb consuming 75 W (Gayral, 2017). This show the LEDs bulbs far more efficient compared to fluorescent bulbs. Group of nitride-III compound widely employed in optoelectronics application due environment friendly semiconductor compound. The physiscal properties of GaN is very hard material, mechanically stable, wide bandgap semiconductor material with high thermal conductivity suitable for the optoelectronic application.

Constant study on blue to violet LEDs development gives new prospects for consumers to have a better experience and greater value. In optoelectronic, the foremost substrate used in LED manufacturing are SiC and sapphire material. Comparing in terms of cost per 2-inch wafer, silicon substrate is the cheapest followed by sapphire (Krost & Dadgar, 2002). Silicon wafers have a low cost, but high lattice mismatch between GaN and silicon

resulting in high dislocation density in epitaxial layers; (Ayers et al., 2016).

Furthermore, the substrate often suffers from tensile stress during the cooling at room temperature owing to the high thermal expansion coefficient mismatch. Now, however, GaN substrates are gaining attention among researchers in LED field (Seong et al., 2014).

Generally the current density of LEDs on GaN is 5 times higher than LEDs on sapphire (Neumark et al., 2007). The GaN wafer is considered a native substrate for epitaxial GaN growth; native substrate has tremendous advantages.

Therefore, remarkable improvements in quality of the crystalline growth structure of GaN growth is achieved due to the same crystal lattice (zero mismatch). In addition, the similar thermal coefficient will help to achieve non-stress effect between GaN-on-GaN layer. Crystal lattice and thermal coefficient similarity provide less dislocation density level. The optical refractive index difference is zero between the thin film and substrate. Therefore is no reflection of light between the epitaxial layers and substrate subsequently produces high light extraction efficiency. GaN-on-GaN shows high external quantum efficiencies compared to GaN grown on a foreign substrate. Overall, GaN-on-GaN gives unprecedented output density, (Nakamura & Krames, 2013) simplified LED architectures (short process flow), high performance and overall lower cost. The cost for GaN substrate is the major is for the development of GaN. Through continuous development of GaN substrates such as epitaxial lateral overgrowth (ELO), the low-temperature buffer layer, high nitrogen pressure solution (HNPS) method, hydride vapour phase epitaxy (HVPE), ammonothermal crystal growth and Na-flux method has obtained to produce lower wafer cost (Paskova et al., 2010). However, the cost of GaN-GaN wafers are equivalent to about 5 to 10 foreign substrate based-LED based on lumen leads to enormous cost saving (Krames, 2013). In short migration to homogeneous (GaN-on-GaN) compared to heterogeneous epitaxial growth LEDs will better choice in near future due to high IQE, less crystal defect

and high brightness on similar active layer (MQW). Once the production cost for bulk GaN reduced, huge demand on GaN-on-GaN LEDs.

1.2 Objectives of the Present Investigation

Due to unprecedented performance of GaN-on-GaN LEDs provide varies application in LEDs world, the growth optimization of GaN-on-GaN LED at blue emission peak wavelength (450 nm) is the main focus in this study. Optimizing of GaN epitaxial layers grown on native substrate, bulk GaN substrate using orientation of (0001) *c*-plane via metal organic chemical vapor deposition, MOCVD, starting with:-

- (a) n-GaN
- (b) MQWs with InGaN/GaN 6 pairs for QW/QB layers at 450 ± 10 nm via PL/EL emission
- (c) p-GaN

Characterize and analyze epitaxial layer crystalline structure, surface morphology, electrical properties, and optical using the atomic force microscopy (AFM), x-ray powder diffraction (XRD), field emission scanning electron microscopy (FESEM), secondary-ion mass spectrometry (SIMS), hall effect, cathodoluminescence (PL), Photoluminescence (PL), and electroluminescence (EL). Table 1.1 shows the basic requirement to establish GaN-on-GaN blue LEDs on wafer level.

Table 1.1: Targets of the 12 key parameters of GaN Epitaxial Growth

Layer	Properties	Target (GaN Substrate)
Unintentionally doped (Un-GaN) on GaN substrate	Growth rate	$\geq 2.5 \mu\text{m/hr}$
	On-axis x-ray rocking curve value	$\leq 100 \text{ arcsec}$
	Off-axis x-ray rocking curve value	$\leq 150 \text{ arcsec}$
	RMS roughness (AFM)	$< 1 \text{ nm}$
n-GaN	Silicon concentration	$\geq 5 \times 10^{18} \text{ atom/cm}^3$
	Mobility	$\geq 150 \text{ cm}^2/\text{Vsec}$
	Resistivity	$\leq 20 \text{ ohm/sq}$
	RMS roughness	$< 1 \text{ nm}$
MQWs	Blue light emission (PL or CL)	$450 \text{ nm} \pm 10 \text{ nm}$
Mg-doping	Mg concentration	$\geq 1.0 \times 10^{19} \text{ atom/cm}^3$
Working LED with blue emission	L-I-V Result	$L \geq 1 \text{ mW}, I = 20 \text{ mA}, V \leq 8 \text{ V}$
	Spectrum result from EL	$450 \text{ nm} \pm 10 \text{ nm}$

1.3 Scope of the Thesis

The motif of this study is to optimize growth condition and develop the GaN-on-GaN blue LED using native bulk GaN substrate. Before the actual work is carried out, review of nitride-III group important in LEDs, plane comparison of polar *c*-plane GaN vs sapphire and a brief study on the history of GaN-based Blue LEDs is presented in Chapter 2. Apart from this, works that have been done in this field are also presented.

Chapter 3 presents the experimental materials and methodology of reactor used inclusive of metal organic chemical vapor deposition, MOCVD, the material, and growth condition of *c*-plane bulk substrates. Followed by characterization and measurement used this study.

Chapter 4 focuses on the growth and defect characterization on *c*-plane GaN. The defect analysis started with undoped-GaN, follow with n-type and MQWs.

Chapter 5 provides a detailed and basic requirement to establish a GaN-on-GaN of blue LEDs.

Chapter 6 demonstrates the first GaN-on-GaN blue LEDs in Malaysia as effort to become LEDs leader in research and technology provider in the near future. Even though the GaN-on-GaN LEDs research extensively done outside Malaysia. Malaysia well known for among the important electronic/semiconductor player in the world. As per of this

direction, this project was started to establish an optoelectronic research ecosystem in Malaysia.

Chapter 7 shows and explain the sapphire growth condition may not be applicable on bulk GaN substrate. The growth details of bulk GaN substrate towards peak wavelength shift from the desired target value gives a great proof.

Chapter 8 briefly summarizes the work done in this dissertation and also provides future directions for GaN-on-GaN LEDs in Malaysia.

University of Malaya

CHAPTER 2: LITERATURE REVIEW

2.1 Introduction

Silicon very synonym as semiconductor material used in microelectronics, photovoltaics and etc. Silicon from group IV has atomic number of 14. If a material falls between a conductor (such as copper) and an insulator, (such as glass) in terms of electrical conductivity is called semiconductor. A semiconductor material may consist of single type atom or more, such silicon from single atom type, whereas GaN (gallium nitride) and etc are material from more than single atom type called compound material. There are variety groups combination in periodic table with respect to valence electron such as I-VII, IV-VI, V-VI and more. In additional, the latest interest in III-V used in light-emitting diodes begin since 1990s (Gil, 2014).

2.2 Nitride-III group

There are many reasons III-Nitrides or III-V compound interested by the current researcher. The wide direct band gap energy covers from prior than infrared to beyond ultraviolet in the electromagnetic spectrum region compared to other group compound combination as shown in Figure 2.1. Examples of III-V compound such as binary compound GaN, AlN, InN, ternary compound InGaN, AlGaN, and quinary compound InAlGaN. The solid-state device light emitting source called LEDs or LDs are small form factor, high brightness and unprecedented device performance towards energy saving. In terms of commercial applications such as solid-state lighting, backlighting, decorative lighting, automotive lighting, plant growth, indoor lighting, water purification, medical devices and more.

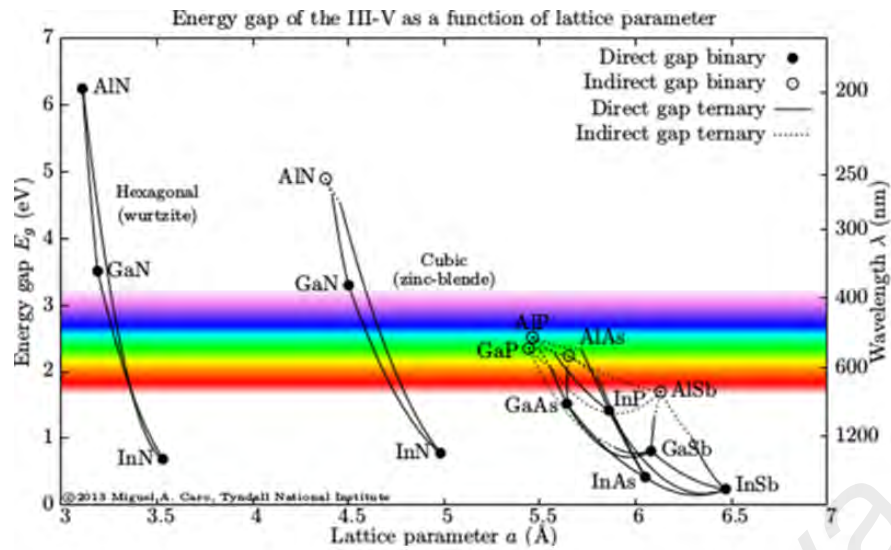


Figure 2.1: Bandgap energy vs lattice constant for typical semiconductors (Bayo, 2013)

2.2.1 Crystal structure and properties of III-V

In this study, only binary GaN and ternary InGaN will be considered. Based on GaN material has unique properties such as very hard material at 12 ± 2 GPa, (Rais-Zadeh et al., 2014) and high thermal conductivity at 253 KW/mK (Shibata et al., 2007). Even though there are 2 two crystal structures consisted of wurtzite and zinc blende, however, wurtzite is the most thermodynamically stable structure stable crystalline structure of AlN, GaN and InN semiconductors compound under ambient conditions (Bayo, 2013). The crystal structure of wurtzite and zinc blende is hexagonal and cubic structure respectively. The wurtzite structure was chosen in this study. Figure 2.2 shows the GaN unit cell structure. The GaN material has tetrahedral bonding structure.

Even though, the GaN material made from covalent bonding. However due to the high difference in electronegativity on N atom cause the electron density from GaN atom attracted to it. This creates an ionic character in covalent bonding about 38% (Carter & Norton, 2007). The GaN material has tetrahedral bonding structure. The stacking sequence of a hexagonal close-packed structure is ABABAB... The GaN material stack

such GaNGaNGaN... in the direction of [0001]. Since there is lack of inversion symmetry in the (0001) plane this will generate a dipolar moment as shown in Figure 2.2. Whereas in Figure 2.3 shows the dipole moment direction it is opposite to [0001] direction due to lack of inversion symmetry.

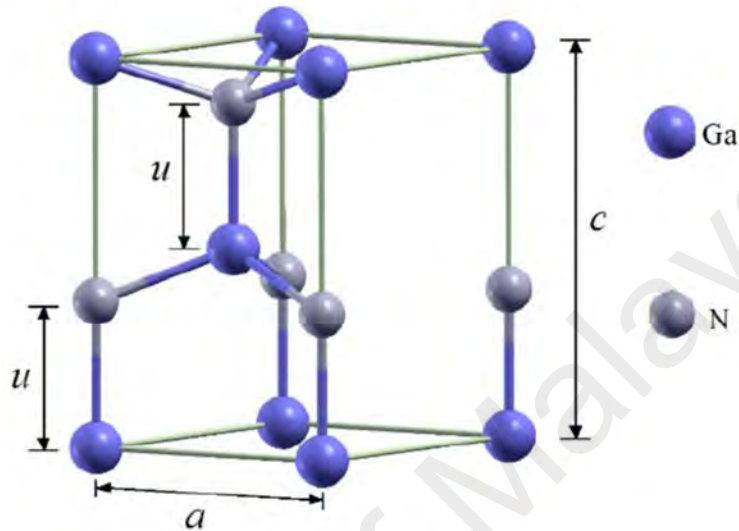


Figure 2.2: GaN unit cell structure (Miguel et al., 2014)

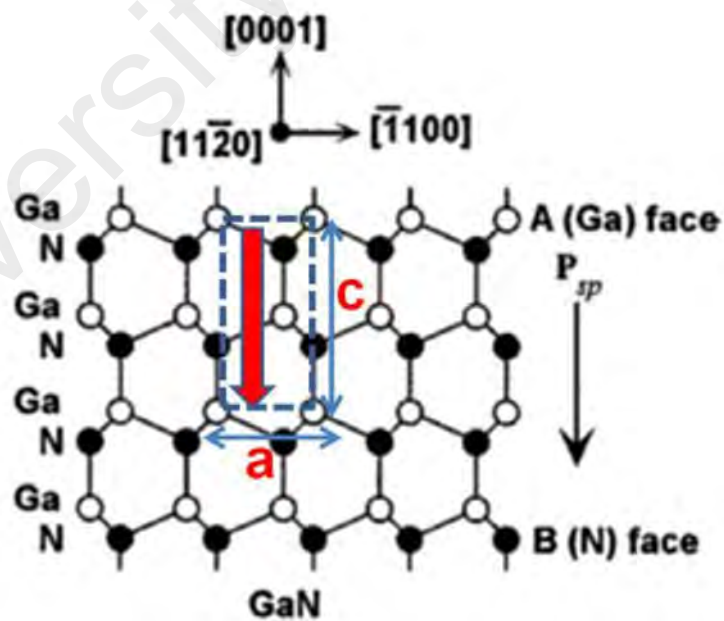


Figure 2.3: Crystal structure for GaN, with unit cell (blue dashed line), dipole moment (red arrow) and lattice parameters a and c denoted in red (Ren, 2016)

Since the c -plane effected by the dipole moment, hence the c -plane called polar plane and beside another plane called semipolar and nonpolar. The Figure 2.4 shows the respective Miller indices for each different plane orientation. The c -plane direction pointed out from the paper. Basically, the crystal orientation can be classifying into 3 categories they are polar (c), semipolar (r), and nonpolar $m(a-$ and $m-$).

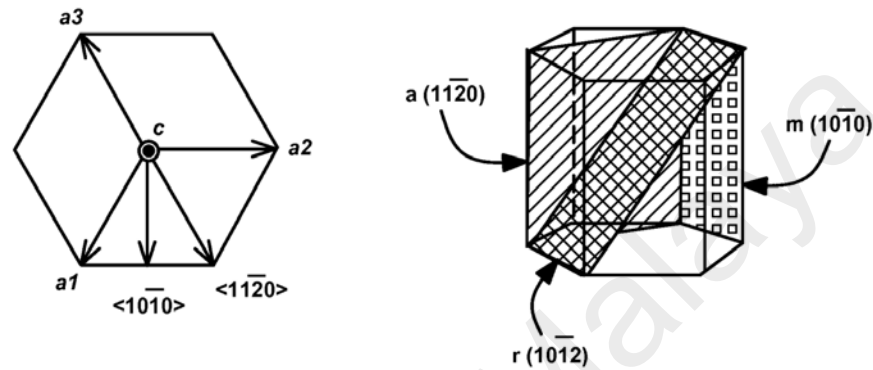


Figure 2.4: Wurtzite structure, left: Miller indices for, right: Orientation of a-,m-, and r- (Imer et al., 2012)

2.2.2 Energy band

Energy gap, E_g is the band separate the upper band (conduction band) and lower band (valence band). Sometimes is gap called a "forbidden band", since in a perfect crystal it contains no electron energy states at 0 K. From the band diagram, one can categorize into a direct and indirect semiconductor as shown in Figure 2.5. There are 2 curves, upper and lower curve. The upper curve is higher energies band, whereby the lower curve called lower energies band. There are many overlapping bands in k -space however, minimum gap is taken as E_g . During falls of higher energy of a electron from convection band to valence releases energy in form of photon equal to E_g . For indirect semiconductor energy will may partially converted to lattice vibration and heat.

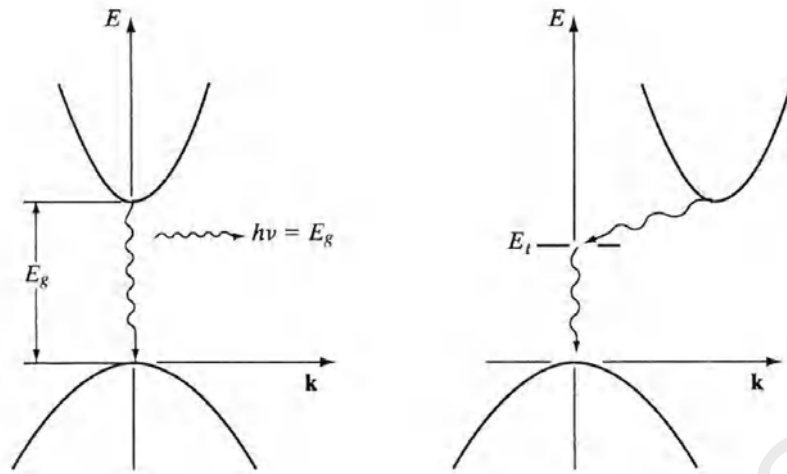


Figure 2.5: Left: Direct band gap, Right: Indirect band gap (Gupta et al., 2015)

Subsequently, if two material stacks such as the GaN/InGaN pair layers it is called MQWs. Provided the each thickness layers are in few nanometers. Desired band diagram for MQWs of InGaN/GaN shown in Figure 2.6. The bandgap of the well material is denoted E_g and the energy of the ground state transition is denoted E_1 .

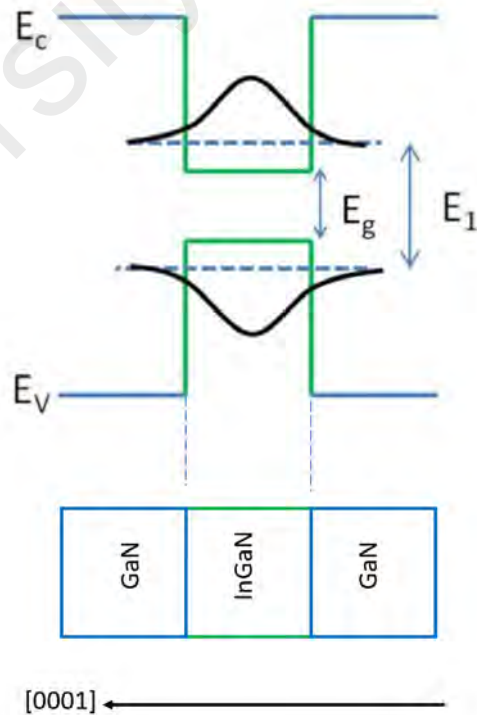


Figure 2.6: Band diagram of MQWs, GaN/InGaN/GaN (Ren, 2016)

2.2.3 Polarization and Stack effect

The wurtzite crystals is lacking an inversion center (non-centrosymmetric) which exhibit the macroscopic polarization in the crystal. The total polarization is the sum of the spontaneous and piezoelectric polarization components. The spontaneous polarization is an intrinsic property of the material. The origin of the spontaneous polarization is the deviation from an ideal tetrahedral coordination along the (0001) axis for the III-nitride wurtzite crystal and the ionicity of the crystal (the difference in respective electronegativities of the two elements forming a bond). As a result of these conditions, each unit cell exhibits a non-zero dipole moment as shown schematically in Figure 2.2. For an ideal hexagonal closed packed crystal with zero spontaneous polarisation, the ratio of the lattice parameters c_0 and a_0 , if all the nearest neighbour bond lengths are equal given by 1.63. If a hexagonal closed packed crystal obtain a less or more will exhibit the spontaneous polarization. As the c/a ratio decreases, the angle between the three bonds at the base of the tetrahedral bonding structure increases, causes a lower compensation polarization along the c -axis and an enhanced spontaneous polarization (Ren, 2016). The piezoelectric polarization is caused by strain in the material, which essentially changes the c/a ratio in wurtzite nitrides. The direction of the polarization vector is always parallel the c -axis in wurtzite crystals and positive polarization is defined the same as the positive [0001] direction. Current semiconductor technology makes extensive use of heterostructures, the joining of materials with different compositions. It is beneficial for the two materials to have closely related crystal structures and lattice constants, however, exact matching is usually not possible. Thus the thinner layer, a quantum well (QW) for example, is strained to match the lattice constant of the bulk material. The piezoelectric polarization component is generated by the strain of the layers (different intrinsic spontaneous polarization). Piezoelectric polarization discontinuities cause band bending as illustrated in Figure 2.7 and result in the quantum

confined stark effect in quantum wells, (QCSE).

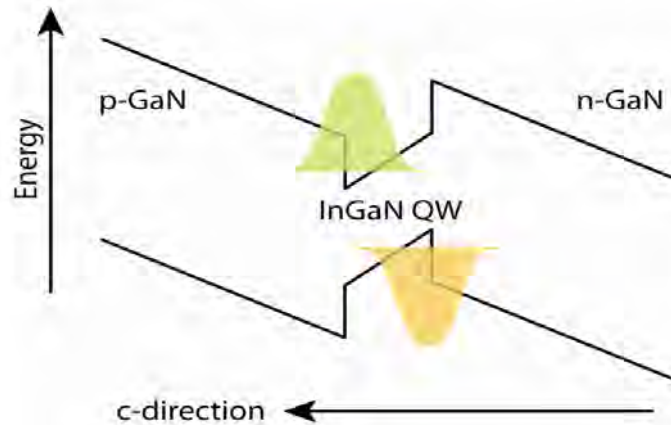


Figure 2.7: Influence of polarization induced electric field (Speck & Chichibu, 2009)

The conduction band and valence band are bend due to the internal electric field. This reduces the overlap of electron and hole wave functions. The consequences of this effect are decreased the recombination efficiency drops the internal quantum efficiency, IQE (Feezell & Nakamura, 2018). The net polarization discontinuity increases as the indium composition is increased in InGaN QWs with GaN barriers (Ren, 2016).

2.3 Nucleation and growth

During classical growth from gas-phase on heterogeneous substrates three different growth modes can take place:-

- (a) Island (Volmer-Weber, VW) growth occurs when the deposited atoms are stronger than those of the atoms with the surface, leading to the formation of three-dimensional atom clusters or islands (Evans et al., 1996);
- (b) Layer-by-layer (Frank-Van der Merwe, FM) growth mode occurs when stronger atoms-substrate bonding leads to planar, layer by-layer deposition (Copel et al., 1989);

(c) Stranski-Krastanov, mode is a combination of the previous two. The latter starts with several complete monolayers and continues with 3D island growth as layer by-layer growth becomes energetically unfavorable. When growing semiconductor materials for electronics and optoelectronics, such as GaN, it is a requirement to obtain single crystal epitaxial films, therefore growth parameters must be adjusted so that layer-by-layer growth takes place (Mo et al., 1990).

The criterion for a film growth mode is dependent on $\frac{d\mu}{dn}$ (Markov, 1995). The VW growth: $\frac{d\mu}{dn} < 0$ (atom cohesive force is stronger than surface adhesive force). Whereas the FM growth: $\frac{d\mu}{dn} > 0$ (surface adhesive force is stronger than atom cohesive force). Where $\mu(n)$ is the layer chemical potential per atom. Even though GaN-on-GaN is a homoepitaxial growth process, the basic nucleation and heteroepitaxial techniques are essential to know and understand.

2.4 Defect related to GaN epitaxial

All real crystals contain imperfections which may be point, line, surface or volume defects, and which disturb locally the regular arrangement of the atoms. Their presence can significantly modify the properties of crystalline solids, and although this text is primarily concerned with the line defects called dislocations, it will be seen that the behavior and effects of all these imperfections are intimately related

(a) Point defects- There are two types of point defect are possible, namely a vacant atomic site or vacancy (the vacancy has been formed by the removal of an atom from an atomic site), and a self-interstitial atom. The vacancies and interstitials can be produced in materials by plastic deformation and high-energy particle irradiation. Impurity atoms in a crystal can be considered as extrinsic point defects and they play an important role in the physical and mechanical properties

of all materials. The impurity atoms can take up two different types that are substitutional (an atom of the parent lattice is replaced by the impurity atom) and interstitial (the impurity atom is at a nonlattice site similar to the self-interstitial atoms)

- (b) Line (called dislocations)- Atoms of the crystal lattice are misaligned. There are two basic types of dislocations that are the edge and the screw dislocation. Generally the edge, screw and mixed will create the threading dislocation which known as line defect.
- (c) Planar or surface defects- There are few types of planar defects mainly focused to grain boundaries and stacking faults.
- (d) Bulk or volume defects- Three dimensional macroscopic or bulk defects, such as pores, cracks, or inclusions. The voids (bubbles) is a small regions where there are no atoms, and which can be thought of as clusters of vacancies. Impurities can cluster together to form small regions of a different phase. These are often called precipitates.

2.5 GaN-on-GaN LEDs performance

Bulk-GaN-based light-emitting diodes (LEDs) are attracting more and more attention due to high power and high devices efficiency. The first LEDs grown on bulk GaN substrates were reported by University of California Santa Barbara (UCSB) group in 2005. Over the many years further improve in performance of native bulk-GaN-based LEDs have been demonstrated. In 2007, the violet LEDs InGaN quantum wells (2.5 nm thick) were grown on $(10\bar{1}\bar{1})$ GaN bulk substrates (Tyagi et al., 2007). The external quantum efficiency, EQE of the 411 nm LEDs at 20 mA was 33.91%. In 2011 a blue LED grown on $(20\bar{2}\bar{1})$ GaN bulk substrates with 3 nm thick InGaN quantum wells have an EQE of 52% at 20 mA reported (Zhao et al., 2011). Nichia reported low-output-power (<100 mW) blue LEDs on

patterned sapphire substrates (PPS) with EQE = 85.9% and a WPE = 81.3% on a $450 \times 450\text{-}\mu\text{m}^2$ chip at given 20 mA in 2010. Daniel reported the violet LEDs grown on $(30\bar{3}\bar{1})$

GaN bulk substrates with a single quantum well (15 nm thick) has been demonstrated in 2014 (Becerra et al., 2014). Improvements in light extraction efficiency, LEE and internal quantum efficiency, IQE have enabled violet and blue LEDs with very high EQE and wall-plug efficiency (WPE). A higher power version using a 1 mm^2 chip exhibited an EQE = 76.7% and WPE = 71% at 350 mA ($35\text{A}/\text{cm}^2$) (Narukawa et al., 2010). Sora, Inc. reported a violet (415 nm) LED on a bulk GaN substrate with peak WPE = 84% at 85 °C). Using flip-chip method in 2015 (Hurni et al., 2015).

2.6 GaN epitaxial layer on polar *c*-plane bulk GaN vs sapphire

Even though polarization present in bulk GaN substrates *c*-plane. However, it is a great start for non-polar bulk GaN substrates growth in the future due to cost is higher than polar bulk GaN. Besides, the positive part of using bulk GaN substrate the lattice and thermal mismatch is zero as compared to other substrates such as SiC or sapphire and etc as shown on Figure 2.8.

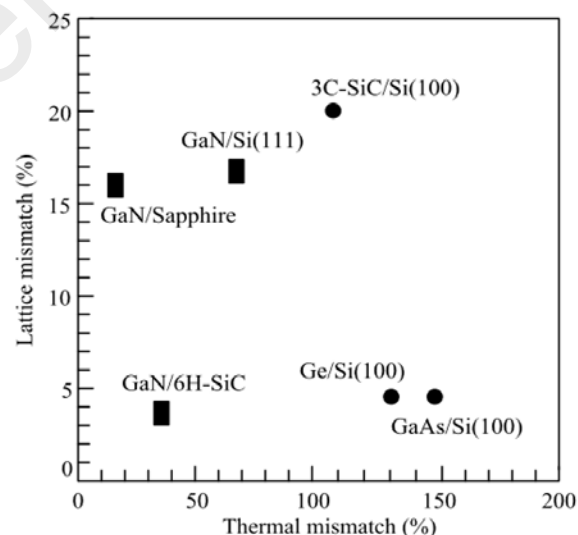


Figure 2.8: Thermal and lattice mismatches in the growth of heteroepitaxy (Nakamura & Krames, 2013)

This will help to minimize the crystal defect compare to sapphire. In general the dislocation density of GaN epitaxial on bulk GaN and sapphire order of 6 and 8 respectively. The TEM image clearly in Figure 2.9 ¹ shows the treading dislocation defect on GaN on Si as compared to GaN-on-GaN which hardly seen.

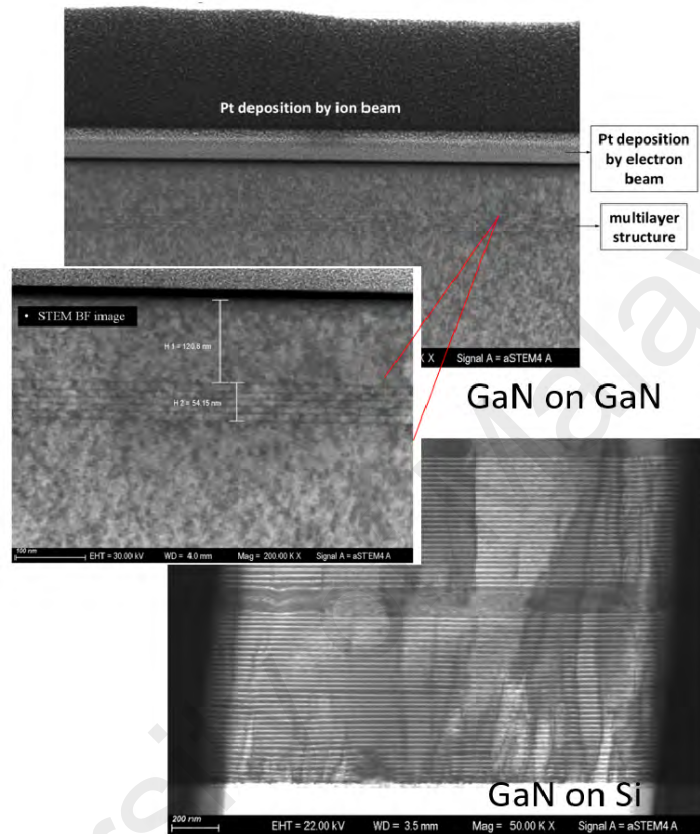


Figure 2.9: Comparison TEM images between GaN-on-GaN and GaN on Si

2.7 A brief history of GaN-based Blue LED research

The semi-conductor group of III-nitrides is widely used in many field light-emitting diodes (LEDs), lasers, ultraviolet detectors and high electron mobility transistors (HEMTs). The early research in semiconductor LEDs can be attributed to Losev, a Russian physicist very talented for creative experimental techniques and observation. However, the first recorded discovery of the LED was by Round in 1907 during his research on SiC crystal detectors for use in the recent phenomenon of wireless radio transmission (Akasaki et al.,

¹ This images from UM sample taken by Carl Zeiss Sdn. Bhd

2014). There was much research seen with LEDs until 1922 when Losev first detected light emission from a silicon carbide point crystal detector. By 1930, Losev had developed theories on p-n junctions and majority carrier injection, but his theory was incomplete due to lack of knowledge on charge carrier type. Losev's discoveries were phenomenal and advance. Since materials for semiconductors were expensive, a perfect crystals were difficult to obtain, and lacked of theory guidance causes research in this field was slow. Creating the theory of light emission from semiconductor diodes only took a few years, and its creation allowed Kurt Lehovec to combine the idea of electroluminescence and diode theory into a coherent theory of LEDs (Lojek, 2007).

Within a few months Lehovec's paper, published in 1952, led to the creation of a p-n junction LED device and hence was born the LED. The first LEDs produced in the 1950s were gallium arsenide based and only emitted the infrared range. As technology began to improve, researchers began attempting to produce LEDs that would emit in all areas of the optical spectrum. However, as LEDs achieved color ranges from red to green, the only blue LEDs known were silicon carbide and gallium nitride. These two compounds are problematic because, until the latter part of the century, they both had notoriously poor efficiencies. Silicon carbide was the first blue LED discovered in the 1920s, but it was not refined until the 1960s. Even by the early 1990s, when the first commercial SiC LEDs hit the market, their efficiency never got higher than 0.03 percentage. This poor efficiency were resulted from SiC's indirect band transition, which led researchers to look for a direct band gap material in the blue end of the spectrum. The production of gallium based LEDs, beginning with the GaAs infrared emitting LED that was discovered in the 1960s, paralleled the development of SiC LEDs. This eventually proved the creation of GaP, and in 1969, (Maruska & Tietjen, 1969) discovered a blue direct transition. Unfortunately, it was very difficult to grow perfect single crystals of GaN at the time, which made p-type

GaN almost impossible to make.

LED displays was being held back by the lack of high-brightness blue LEDs, research was initiated by Nakamura in April, 1989 on the GaN semiconductor system. Further research began to expand in 1992 when Shuji Nakamura developed a thermal annealing method for Mg doped GaN which explained the influence of hydrogen that forms acceptor-H complexes in p-doped GaN film causing hole compensation (Nakamura et al., 1992). Then in 1993, Shuji Nakamura revolutionized the industry with his breakthrough of producing the first prototype high brightness blue LEDs (Nakamura et al., 2013). Since that time, the field of nitride research has greatly expanded, and nitride-based optoelectronic devices are widely commercially available. In 2014 the physics Nobel prize awarded for "The invention of efficient blue light emitting diode" to Akasaki, Amano & Nakamura.

University of Malaysia

CHAPTER 3: EXPERIMENTAL MATERIALS AND METHODOLOGY

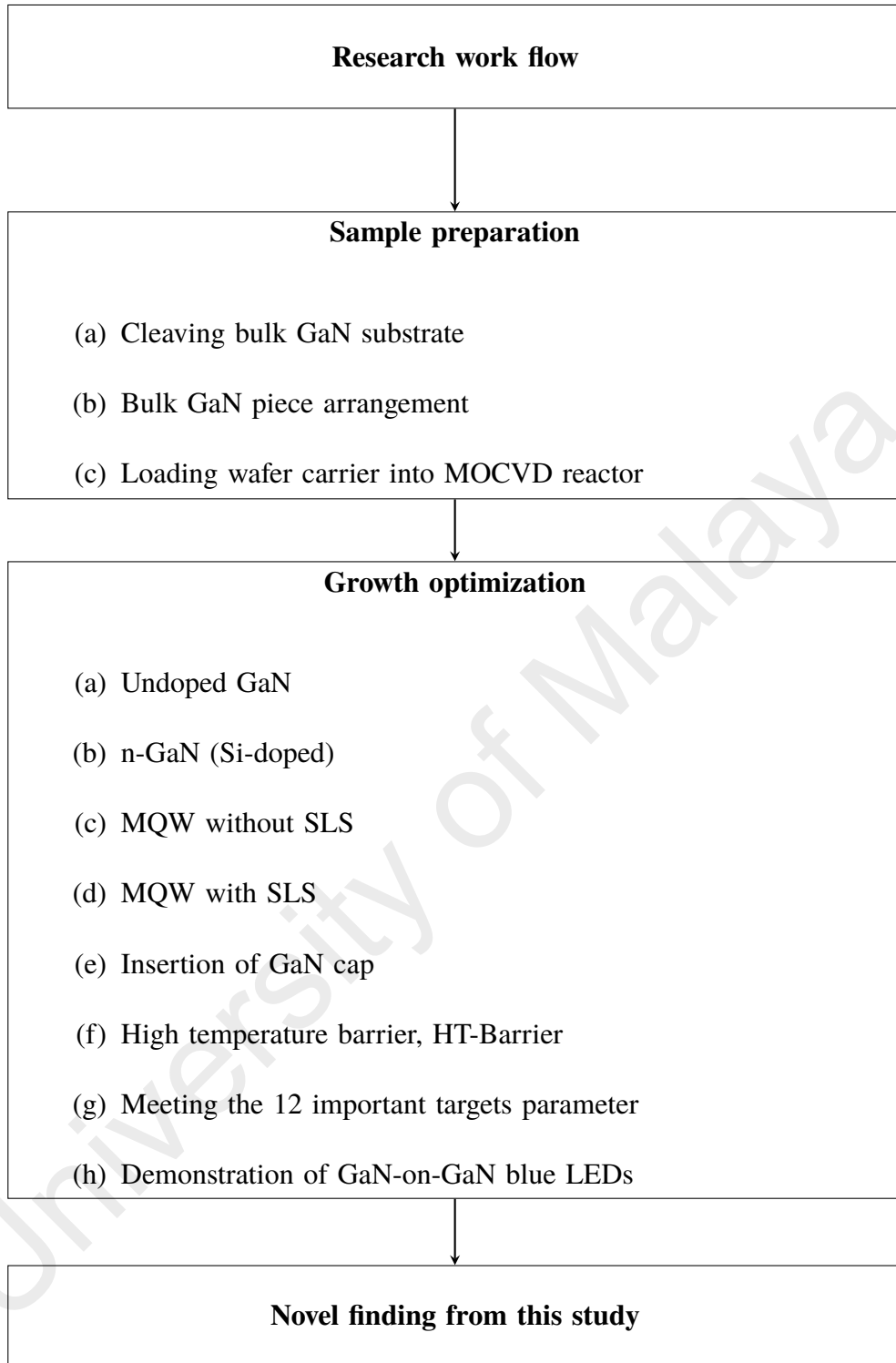
3.1 Introduction

There are older growth techniques such liquid-phase epitaxy (LPE) and chloride vapor-phase epitaxy (CIVPE). This followed by three main growth techniques to produce epitaxial nitride films are metalorganic chemical vapor deposition (MOCVD), hydride vapor phase epitaxy (HVPE), and molecular beam epitaxy (MBE) (Stringfellow, 2012). Each technique has certain advantages and disadvantages. The organometallic vapor-phase epitaxy is often referred to as metal-organic chemical vapor deposition (MOCVD) and by other naming (MOVPE and OMCVD). MOCVD is a epitaxial growth technique which uses metalorganic compounds as the group III source and ammonia as the group V source. This technique is often used to grow device structures with different alloy compositions and doping. This is the technique most commonly used to produce commercial devices.

MBE is a technique which uses an ultra-high vacuum to direct the source materials to the substrate surface. The group III sources are metallic and the group V source is either nitrogen plasma or ammonia. This technique has very slow growth rates, which enable fine control of the composition and the growth of very complex structures.

For HVPE technique, a hydride vapor (HCl) is flowed over metallic gallium from the group III source to form gallium monochloride . HVPE has high growth rates (1 $\mu\text{m}/\text{min}$) and is suitable for growing templates which can be used to grow device structures by MOCVD or MBE.

3.2 Overview of research work



3.3 Metal organic chemical vapor deposition, MOCVD

MOCVD is used to deposit epitaxial layer on substrate by utilizing the volatile metal organic compounds to transport metallic atoms to the reactor. They are called organometallic compounds that usually mixed with other source materials through chemical reaction to form compound semiconductor films. Figure 3.1 shows the diagram of the horizontal flow MOCVD reactor in SR2000 specification. All the group-III and group-V precursor bubblers and gas lines are furnished with the necessary mass flow controllers (MFCs) and pressure controllers (PCs) to control the flow rates of gases during the deposition of materials. The maximum temperature limit of the reactor is 1200 °C. The controllable range of reactor pressure is 10 kPa-100 kPa. The reactor chamber is equipped with the removable quartz ware to prevent the reactor walls from contamination during the growth of materials. Figure 3.2 shows the flow for metal organic, MO sources, NH₃. The H₂ and N₂ gases that used as gas carrier and MO carry to move the MO and NH₃ from the source to the reactor during growth.

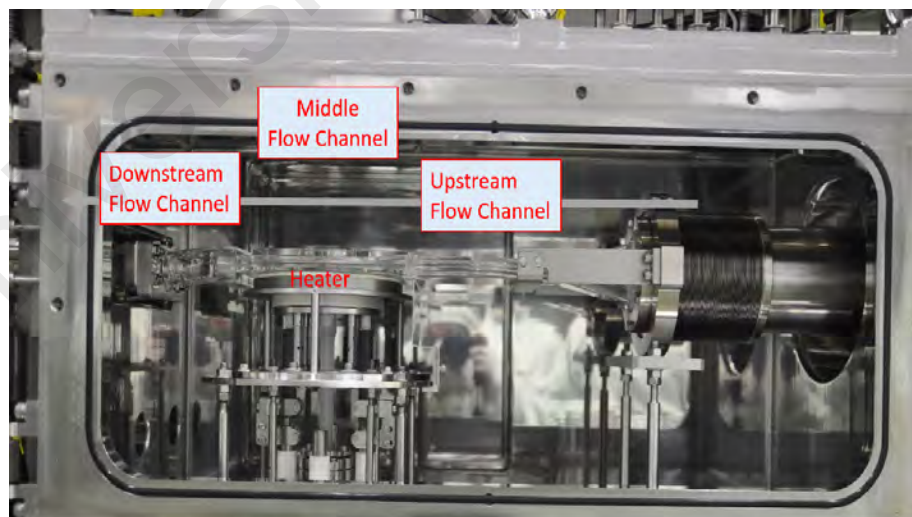


Figure 3.1: Horizontal MOCVD reactor

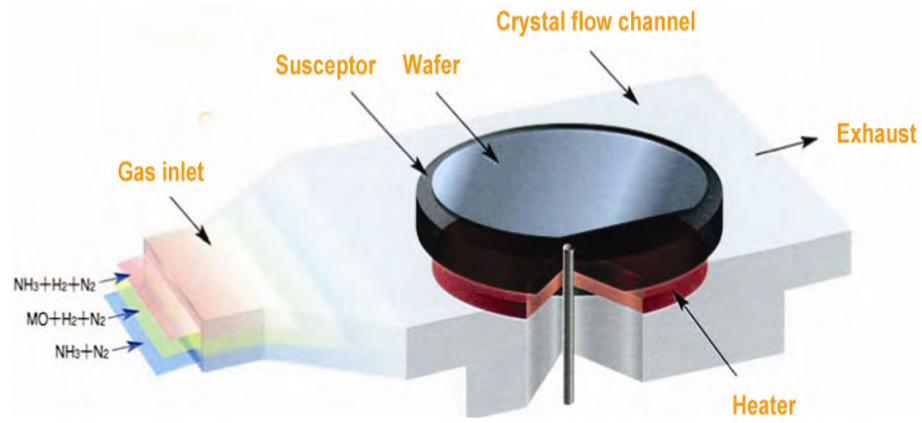


Figure 3.2: Horizontal three-layer laminar-Flow Channel (Matheson, 2015)

Chemical Equation 3.1 shows the trimethylgallium, TMG source dissociates with presence of thermal supplied and hydrogen ambient. Chemical Equation 3.2 shows the ammonia gas (NH_3) dissociates easily around $1000\text{ }^\circ\text{C}$. Due to this, a high-quality GaN can be obtained when the growth temperature is around $1000\text{ }^\circ\text{C}$. Chemical Equation 3.3 shows the overall chemical reaction showing the formation of GaN (epitaxial layer) and methane (CH_4) as the byproduct. Where methane decomposes to carbon and can be seen as black debris during wafer unloading if the exhaust system works inefficiently.



3.4 Material preparation and growth on *c*-plane bulk GaN substrates

3.4.1 Sample preparation

The double side polished (DSP) bulk GaN substrates were prepared by using hydride vapor phase epitaxy growth along the [0001] direction from SCIOCS company limited. The description and specification of bulk GaN substrate given GAN-S-N-T40(51)/M-0.4AOFF-AOF and SP15-25-1169 respectively. Bulk GaN piece was cleaved to a size of $5 \times 5\text{-mm}^2$ and cleaned prior to growth. The cleaning process involved acetone, isopropyl alcohol and deionized water for 15, 15, and 10 minutes respectively in an ultrasonic bath followed by heating in the oven at $110\text{ }^\circ\text{C}$.

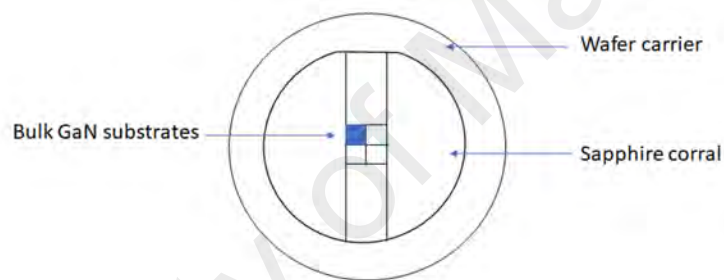


Figure 3.3: Bulk GaN substrates and sapphire corral arrangement on wafer carrier

In order to accommodate the 2-inches wafer carrier size, the sapphire corral is administered surrounding the bulk GaN piece shown as Figure 3.3 on wafer carrier and load manually to MOCVD reactor.

3.4.2 Growth condition

The epitaxial growth was performed by using metal organic chemical vapor deposition (MOCVD). Metal organic (MO) sources were trimethylgallium (TMGa), trimethylindium (TMIn), ammonia (NH_3) and silane (SiH_4) were used as Ga, In, N, and Si sources, respectively. The substrate was initially heated under ammonia flux and subsequently, a silicon doped n-GaN was grown at $1100\text{ }^\circ\text{C}$. The temperature was then ramped down to

697–777 °C to grow InGaN/GaN MQWs structures. There are total 6 pairs of InGaN/GaN MQWs targeted for blue emission at 450 ± 10 nm. In reality the number of active layer (MQWs) pairs varies from 10-20 depends on resistivity and brightness required. As the pair increases the resistivity increases too. This may leads to decrease in device efficiency (Chang et al., 2002). In additional shifts in PL and EL peak positions observed. The growth temperature of the InGaN QWs and the GaN cap layer were grown at the same temperature at 697 °C. The GaN quantum barrier temperature of were varied at 697 °C, 773 °C, and 777 °C. The MQWs structure was terminated with a GaN quantum barrier layer. The V/III ratio for the n-type, QW, GaN-cap and the QB layers are 2161, 12450, 27100 and 7181, respectively. Figure 3.4 is the complete test LED structure had investigated.



Figure 3.4: Left: Basic schematic of the GaN-on-GaN blue LEDs structure, Right: Blue light emission

3.5 Characterization

In this section, brief discuss on the basics of the main characterization methods and experimental setups. Structural characterization of the c-plane GaN optimization series involved surface morphology and crystallography analysis used high-resolution X-ray diffraction (HRXRD), photoluminescence spectroscopy (PL) and more. The principal electrical characterization techniques used here is Hall effect. Scanning electron microscopy (SEM) and FESEM images were recorded using FEI Sirion and JEOL 6300 instruments

respectively. Atomic force microscopy (AFM) images were measured using a Digital Instruments D3000 tool. Transmission electron microscopy (TEM) characterized using an FEI Tecnia G2 Sphera microscope at an operating voltage of 200 kV. In addition, the combined effect of run-to-run variability in MOCVD process should be taken into account. To maintain consistency of MOCVD reactor, the reactor conditions were monitored while followed the same conditioning and bake routine before each growth period.

3.5.1 Analyzing structural and optical properties

(a) High-resolution X-ray diffraction, HRXRD.

XRD is ideal for III-nitride characterization due to its non-destructive nature, high strain sensitivity, rapid analysis and representative results (Moram & Vickers, 2009). The basis of Bragg's law, which relates the spacing between the 'planes' of atoms from which diffraction is occurring with d-spacing at specific angle (θ) at which the incident monochromatic beam must probe the plane to give constructive interference given by Equation 3.4.

$$n\lambda = 2d\sin\theta \quad (3.4)$$

(b) Field emission scanning electron microscope, FESEM

The FESEM provides topographical and elemental information at magnifications of 10x to 300,000x, with virtually unlimited depth of field. As compared with convention scanning electron microscopy (SEM), field emission SEM (FESEM) produces clearer, less electrostatically distorted images with spatial resolution down to 1.5 nm – three to six times better. The principle of operation by using field-emission cathode in the electron gun of a scanning electron microscope provides narrower probing beams

at low as well as high electron energy, resulting in both improved spatial resolution and minimized sample charging and damage (Brodusch et al., 2017).

(c) Secondary-ion mass spectrometry, SIMS

A technique used to identify the types of atom present, analyze the composition of solid surfaces and thin films by sputtering the surface of the specimen with a focused primary ion beam and collecting and analyzing ejected secondary ions (Van der Heide, 2014).

(d) AFM

An AFM images the topography of a sample surface by scanning the cantilever over a region of interest. The raised and lowered features on the sample surface influence the deflection of the cantilever. By using a feedback loop to control the height of the tip above the surface—thus maintaining constant laser position—the AFM can generate an accurate topographic map of the surface features (Haugstad, 2012).

(e) Photoluminescence (PL), Cathodoluminescence microscope (CL) and Electroluminescence (EL)

Photoluminescence is a spontaneous emission of light under optical excitation. Incoming photons with energy larger than the material band gap are absorbed by the sample. The absorbed photon creates an electron-hole pair inside semiconductor that recombines rapidly emitting another photon. The energy of emitted photon depends on the material properties and is approximately equal to the band gap of the sample. Cathodoluminescence (CL) microscope is designed to study the luminescence characteristics of polished thin sections of solids irradiated by an electron beam. CL is

capable of measuring the local density of states (LDOS) of a nanostructured photonic medium, where the intensity of the emitted CL reflects directly the number of available photonic states. Electroluminescence (EL) is usually performed on the finished devices (such as LEDs) since it needs a device structure to inject current (Kumar, 2013).

3.5.2 Electrical characterization

(a) Hall effect

The hall effect is the production of a voltage difference (the Hall voltage) across an electrical conductor, transverse to an electric current in the conductor and to an applied magnetic field perpendicular to the current (Popovic, 2003)

CHAPTER 4: RESULTS AND DISCUSSION: DEFECT ANALYSIS ON C-PLANE GaN

4.1 Introduction

According to Nobel laureate's winner (Shuji), LEDs can be categorized mainly into two types, that is the heteroepitaxy growth called the first generation LEDs and homoepitaxy growth called the second generation LEDs. In this research study, GaN epitaxy layers with /without doped or III group metals on bulk GaN substrates considered. The quality of crystal important measure to ensure high efficient LEDs produced.

4.2 Growth of Undoped and n-type GaN layer on bulk GaN substrates

Generally, homoepitaxy doesn't require buffer layer if compared to heteroepitaxy due to same lattice structure between the epitaxial layer and substrates. The first layer on bulk GaN growth will be the n-GaN. The n-GaN epitaxial layer thickness typically 1 μm to 2 μm on *c*-plane bulk GaN (Armstrong et al., 2013; Lai et al., 2009). However to grow n-GaN layer, firstly the unintentionally or undoped epitaxial GaN layer (Uid-GaN or Undoped-GaN) needed to be optimized. Figure 4.1 shows the 1st epitaxy layer on bulk GaN substrate via MOCVD. The recipe condition can be seen at appendix A.



Figure 4.1: The first layer on bulk GaN substrates

This to ensure the first layer is very basic and without the influences of dopant towards the epitaxial GaN morphological layer. The undoped GaN thickness used about 1.5 μm . According to Figure 4.2 the RMS roughness value obtained from AFM scan at 0.48 nm

($2 \times 2\text{-}\mu\text{m}^2$ area scan) and the surface looks smoother compared to 0.7 nm ($2 \times 2\text{-}\mu\text{m}^2$ area scan) (Chen et al., 2002). Besides that the and FESEM image show the undoped GaN is smooth surface, however observed some contamination (black spots) at few spots from microscope images suspect due to carbon residual from dissociation of metal organic source during chemical reaction above the substrates surface.

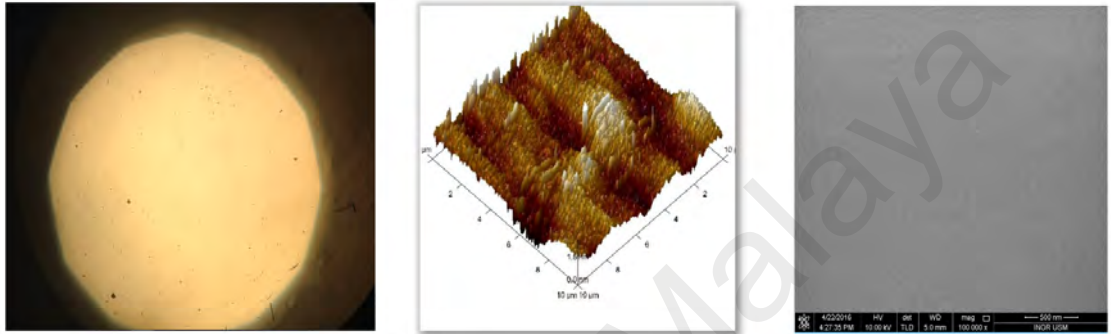


Figure 4.2: Sample G007-Undoped GaN, Left: Surface under image microscope under 200X, Middle: AFM scan image , and Right: FESEM scan image

The n-GaN thickness used is about 2.64 μm . The growth of n-GaN at 18 sccm and 30 sccm silane flow gives 0.4 nm and 0.9 nm respectively for samples G074 and G075. As compared to samples G074, the G075 surface more rougher due to high silane flow as shown on Figure 4.3.

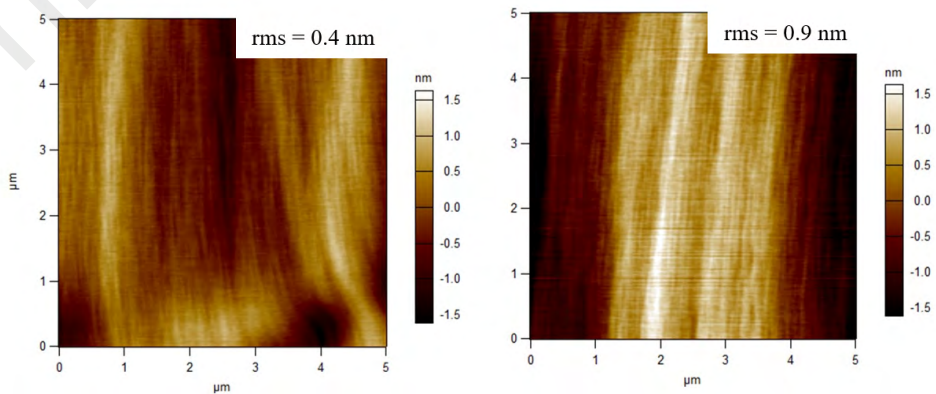


Figure 4.3: RMS of surface roughness, Left: Sample G074, Right: Sample G075

4.3 Insertion n-type strained-layer superlattices, SLS layer

The insertion of strained-layer superlattices, SLS layer before MQWs provided less defect from reduction or elimination of treading dislocation. The pair used here is InGaN/GaN with slight dopand with Si for both QWs and QBs to reduce resistivity. Generally the amount of the In used around 2-3 percentage. According to literature review, the lattice mismatch between InGa and GaN create strain which reduces the strength and redirect the treading dislocation downwards and prevent from further propagate to MQWs (Leem et al., 2008; Quan et al., 2015).

4.3.1 Without SLS

Figure 4.4 shows the MQWs structure with 6 pairs and with each MQW period at 11.1 nm thickness that obtained from XRD from sample G043. The MQWs temperature at 697 °C for both QWs and QBs. The estimated thicknesses of QWs and QBs from HRXRD at 2.4 nm and 8.7 nm respectively. The epitaxial thicknesses of the total repeat an InGaN well plus a GaN barrier obtained using the omage-2 theta measurement from HDXRD on the (002) reflection. Using the value range of arcsec of satellite peaks from -1 to -2 or +1 to +2 (Vickers et al., 2003). With understanding the fact the deposition rate of InGaN and GaN at the particular temperature, the respective thicknesses can be estimated.

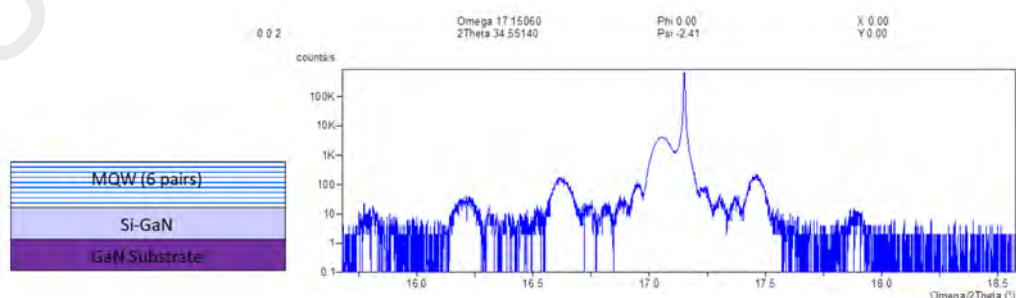


Figure 4.4: Sample G043, Left: Structure without SLS, Right: Omega-2theta from XRD

Figure 4.5 shows the AFM image with $5 \times 5\text{-}\mu\text{m}^2$ scale, with the RMS roughness of 0.83 nm. Whereas the defect density of $1.96 \times 10^8 \text{ cm}^{-2}$ was obtained using manually calculation from defect points within $5 \times 5\text{-}\mu\text{m}^2$ area scan then convert to defect unit to cm^2 . Generally there are 2 distinct spots which is the black and white colour. The red line shows the AFM probe traveled and produces the AFM depth profile. When the AFM probe scan through the interested area (on red line) using AFM depth profile shows in the graph 2 distinct uneven surface that is minimum and followed with maximum function. It shows the black spot is deep inside maybe a v-pits (Sheen et al., 2015) about 17.5 nm (17.5-0) and the other-hand the white spot higher than surface about 15 nm (32.5-17.5) from Figure 4.5 on the right.

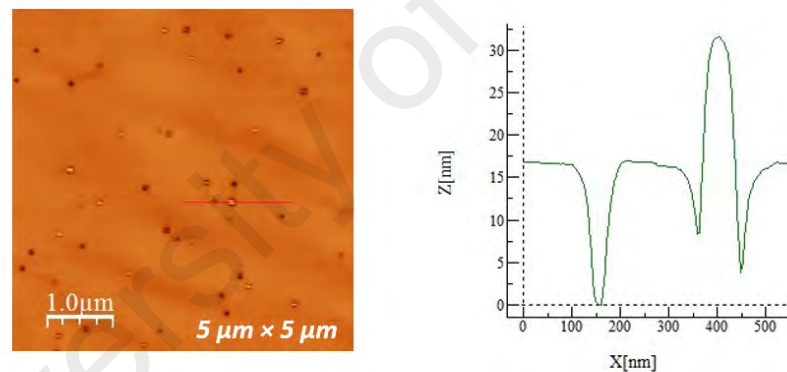


Figure 4.5: Sample G043, Left: AFM scan image on MQWs structure without SLS layer, Right: AFM depth profile

Figure 4.6 shows the CL image. A single treading dislocation in MQWs layer it represented by a small black spot (Choi et al., 2004). However, the larger black spot is a cumulation of many treading dislocations in MQWs layer. Take note the defect density and treading dislocations density are not same. The defect density are due to treading dislocations and surface defect. In order to make a rough estimation of the treading dislocation density, the bigger spots are excluded from treading dislocation spot and

analyzed separately. Hence the threading dislocation density is estimated to be at $6.32 \times 10^7 \text{ cm}^{-2}$. MQWs emission spectrum is important to ensure the growth temperature similar through the SLS study. From CL spectrum shows the peak wavelength at 444 nm.

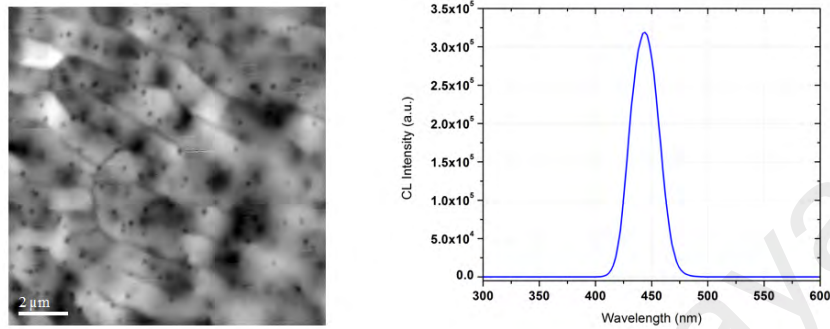


Figure 4.6: Sample G043, Left: CL scan image of MQWs structure without SLS layer, Right: CL spectrum

4.3.2 With SLS

Figure 4.7 shows the SLS structure having 20 pairs on n-GaN. The MQWs is above the SLS layers.



Figure 4.7: Sample G046, MQWs structure with SLS layer

Figure 4.8 shows the AFM scan image of $5 \times 5\text{-}\mu\text{m}^2$ area and the RMS surface roughness value at 0.42 nm. Through manual calculation the defect density from that image at $5.60 \times 10^7 \text{ cm}^{-2}$. The white spot only higher than surface by 4 nm. Comparing the with and without SLS, insertion of SLS helps in reducing term of the defect density and RMS roughness results.

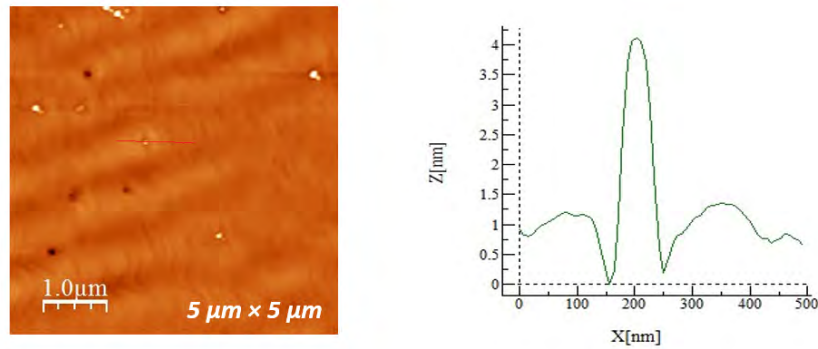


Figure 4.8: Sample G046, Left: AFM scan image AFM scan image on MQWs structure with SLS layer, Right: AFM depth profile

Figure 4.9 shows the CL images. The threading dislocation density is estimated to be $6.22 \times 10^7 \text{ cm}^{-2}$. Even though the approximate improvement is only by 1.6%, it is believed that this figure can be increase with continues recipe optimization of SLS such as number of SLS pairs, silane flux flow and growth temperature. The total tiny and big black spot area obviously lesser if compared to CL image of G043. From CL spectrum shows the peak wavelength at 446 nm almost similar condition G043 growth condition applied. Hence applying the SLS before MQWs growth shows an improvement in threading dislocation towards high quality MQWs structure as shown in Table 4.1. Wavelength shifted by 2 nm considered typical and acceptable.

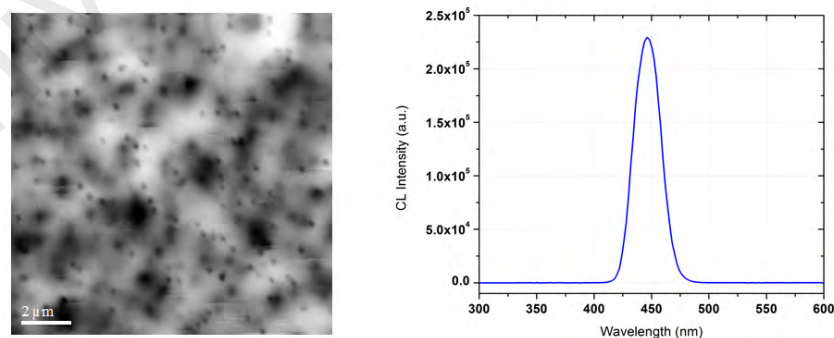


Figure 4.9: Sample G046, Left: CL scan image AFM scan image of MQWs structure with SLS layer, Right: CL spectrum

Table 4.1: With and without SLS comparison

Sample no.	With or without, SLS	Defect density cm^{-2}	RMS, roughness, nm	Treading dislocation density, cm^{-2}	Wavelength, nm
G043	Without	1.96×10^8	0.83	6.32×10^7	444
G046	With	5.60×10^7	0.42	6.22×10^7	446

4.4 GaN cap optimization for higher temperature barrier, HT-Barrier

The indium content of $\text{In}_x\text{Ga}_{1-x}\text{N}$ (QWs) multi-quantum wells (MQWs) for LED devices is highly sensitive to growth temperature (Hu et al., 2012). At higher growth temperatures it increasing the likelihood of indium to be desorbed however, at lower growth temperatures the crystalline quality of the grown material will be affected. Generally indium beings to desorbs at 500 °C and above, which lead to blueshift shift(Hu et al., 2012). Theoretically lesser indium content in the quantum wells will lead to shorter wavelengths. According to Kumar, higher temperature barriers growth reduces the presence of V-pits and subsequently improves the surface morphology of the multi-quantum wells, MQWs pairs (Kumar et al., 2007). To have the HT-Barrier growth, the GaN cap is a vital layer. Usually the GaN cap grown on low temperature or at same as QWs condition. The low-temperature Pre-Cap GaN promotes better growth condition of InGaN QWs growth.

A GaN cap needed to minimize the indium desorption and to ensure temperature independent. Figure 4.10 and Table 4.2 elaborates on the GaN cap thickness optimization. The temperature of QWs and QBs are kept at 697 °C and 777 °C, respectively, and mainly the GaN cap thickness was varied. As the GaN cap thickens, the wavelength is red-shift and saturates. For this growth condition, 45s deposition time is sufficient to maintain the wavelength around 450 nm.

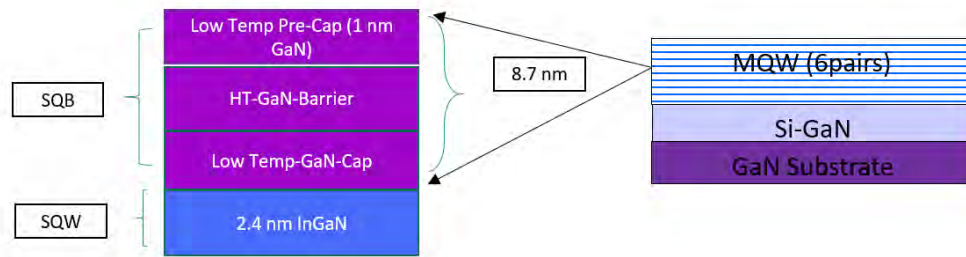


Figure 4.10: Details for MQWs

Table 4.2: GaN cap optimization table

Sample no.	GaN cap time, t/s	HT Barrier time, t/s	GaN Cap thickness, nm	HT Barrier, nm	Total barrier, nm	Wavelength, nm
G047	25	50	1.2	6.5	8.7	420
G053	35	45	1.7	5.9	8.5	440
G052	45	30	2.2	3.9	7	450
G051	60	15	2.9	2	5.8	453

4.5 Higher Temperature Barrier Growth, HT-Barrier

After obtained the optimized GaN-cap with thickness of 2.2 nm, it is a new GaN-cap layer thickness for HT-Barrier. Low temperature barrier at 697 °C for sample no. G054 and the temperature of QWs and QBs are kept at 697 °C and 777 °C respectively for sample G055.

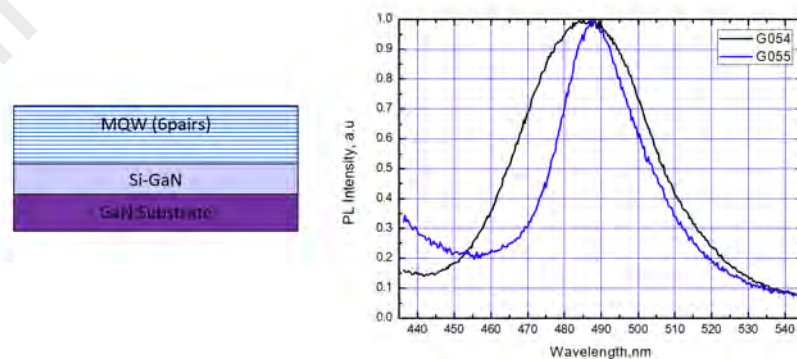


Figure 4.11: Left: MOWs structure, Right: PL spectrum

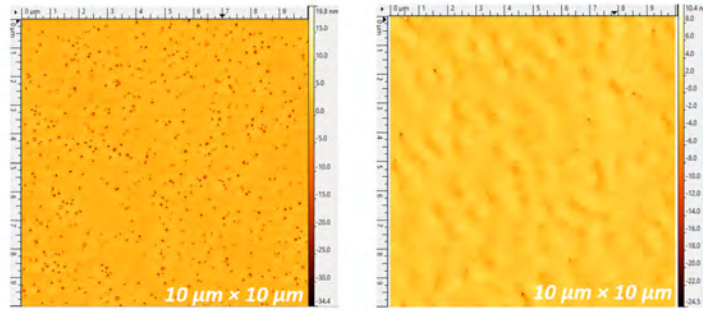


Figure 4.12: AFM image, Left: G054, Right: G055

Sample no. G055 clearly demonstrates an improvement in defect density, spectrum narrowness through HB-barrier growth technique compared to G054. The data from PL spectrum (Figure 4.11) and RMS surface roughness value from AFM measurement (Figure 4.12) collection kept in table 4.3. Data from AFM scan observed 92% improvement in defect density from $1.67 \times 10^8 \text{ cm}^{-2}$ to $1.30 \times 10^7 \text{ cm}^{-2}$ on G054 and G055 respectively. Moreover the RMS surface roughness show reduction by 60% using the HT-barrier compared to LT barrier condition. Similar growths condition were applied on G054 compare to G043, however the their peak wavelength has significant difference. Based on the desired peak wavelength it should be around 450 nm, however this is not true. Highly suspect it may due to the reactor temperature shifted. In term of FWHM (PL measurement) found the wavelength spectrum become more narrower from 42 nm to 30 nm of sample G055 compared to G054. This may due to the high quality crystal of MQWs with less defect density and smoother surface.

Table 4.3: Comparison between LT (697 °C) and HT (777 °C) barrier condition

Sample no.	Defect Density, cm^{-2}	RMS roughness, nm	Peak wavelength, nm	FWHM, nm
G054	1.67×10^8	2.49	485	42
G055	1.30×10^7	0.99	488	30

4.6 Summary

Based on insertion of SLS 71% and 49% of improvement on defect density and RMS surface roughness respectively. Compared to introduction of HT-barrier technique found that 92% and 60% of improvement on defect density and RMS surface roughness respectively. Even though applying the SLS insertion and HT-barrier shows improvement in crystal quality, which lead to higher efficient LEDs. However compared to these 2 methods approaches the HT-barrier growth technique much is a effective method in improving crystal quality.

University of Malaysia

CHAPTER 5: RESULTS AND DISCUSSION: BASIC TARGET OF BLUE LED

5.1 Introduction

The growth of blue GaN-on-GaN LED by optimizing the each GaN epitaxial layers starting with basic structure of n-GaN followed with 6 pairs MQWs QW/QB InGaN/GaN layers, and lastly the p-GaN grown on the native substrate, bulk GaN substrate with an orientation of (0001) c-plane using metal organic chemical vapor deposition, MOCVD. Figure 5.1 on left shows a typical GaN-on-GaN LEDs structure. The optimization previous chapter.



Figure 5.1: Left: Schematic of GaN-on-GaN LEDs structure , Right: Blue light emission

5.2 Performance Target for Epitaxial Growth

In order to establish the basic wafer form LEDs, generally certain parameters needed to taken into consideration such as crystal quality from XRD, and AFM. Electrically from Hall effect and overall from EL measurement. The SIMS provides a precise growth rate measurement and dopant concentration. Optically CL, PL, and EL provide the optical properties of LEDs.¹ Even the FWHM from optical spectrum able to express quality level of the crystal too. Hence the crystal quality, electrical and optical properties are depends on each another. Referred to Figure 1.1 from chapter 1 liberates the most 12-important

¹ SIMS, XRD, CL data was performed by UCSB, otherwise will be specified

parameters required for basic growth of GaN-on-GaN blue LEDs. Following are the evidences of data measurement and analysis to ensure meet each target requirements.

5.2.1 Data and analysis

(a) Growth rate

To get the growth rate value accurately the best way to obtain is either from the HR-XRD or SIMS, since it is homoepitaxial growth, to acquire from the XRD is difficult. Hence SIMS measurements were used here. A series of stack grew with different of silane flow rates in the sccm unit, (SiH_4) gas. The silane flow used at 18 and 30 standard cubic centimeter/minute (sccm) respectively.

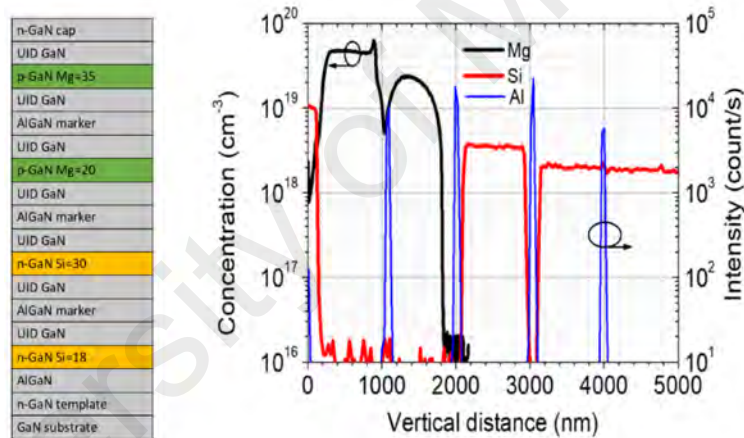


Figure 5.2: Sample G060₃, Left: SIMS stack series, Right: SIMS result

Both n-GaN stacks grown at 15 minutes deposition time, refer to Figure 5.2. If 800 nm thickness of n-GaN at 15 minutes for G060₃ growth time at 30 sccm, then the growth rate at 3.2 $\mu\text{m/hr}$. Same goes to samples G074 and G075 for 30 minutes referring to Figure 5.3. Table 5.1 is the growth rate summary for samples G060₃, G074 and G075. The growth rate of n-GaN shouldn't be too fast or too slow. If its too fast affects the epitaxial crystal quality and morphological of the layer, if its too slow will cause more resources and processing time.

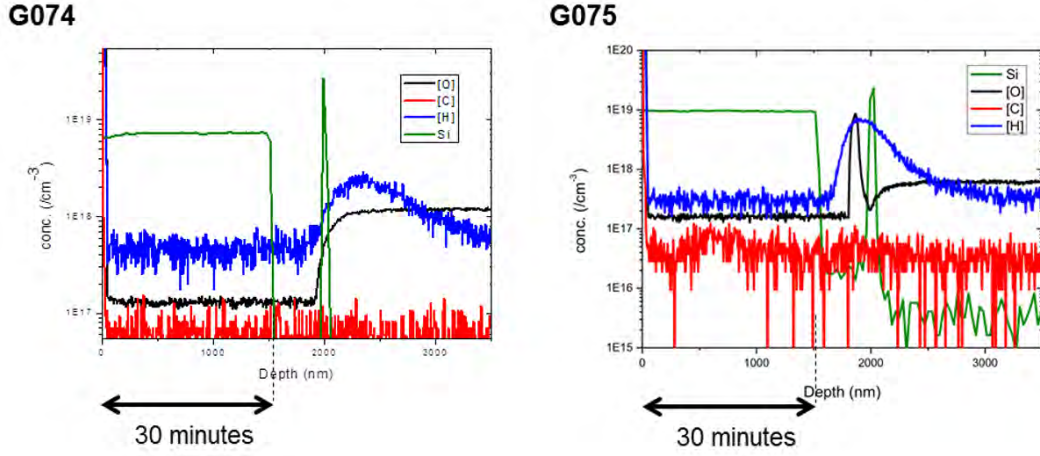


Figure 5.3: SIMS results, Left: Samples G074, Right: Samples G075

Table 5.1: Growth rate of n-GaN

Sample no.	Growth rate ($\mu\text{m/hr}$)
G060 ₃	3.2
G074	3.0
G075	3.0

(b) On-axis x-ray rocking curve value ²

Figure 5.4 below displays the omega scan of 002 plane of undoped GaN; FWHM are 69 and 96 arcsec for samples G007 and G008 respectively. It is noteworthy to mention that 002 peak is broadened by screw dislocations, which can be calculated as (Moram et al., 2009), (Shang et al., 2015)

$$N_{screw} = (FWHM_{002})^2 / 9b_{screw}^2 \quad (5.1)$$

$$N_{edge} = (FWHM_{102})^2 / 9b_{edge}^2 \quad (5.2)$$

where N_{screw} is the screw and N_{edge} is the edge dislocation density and b is the burger vector ($b_{screw} = 0.5185 \text{ nm}$) and ($b_{edge} = 0.3189 \text{ nm}$) respectively (Öztürk et al., 2010). Therefore, the total dislocation density (N_{total}) can be calculated as

$$N_{total} = N_{screw} + N_{edge}.$$

² (002) scan taken from Uid-GaN

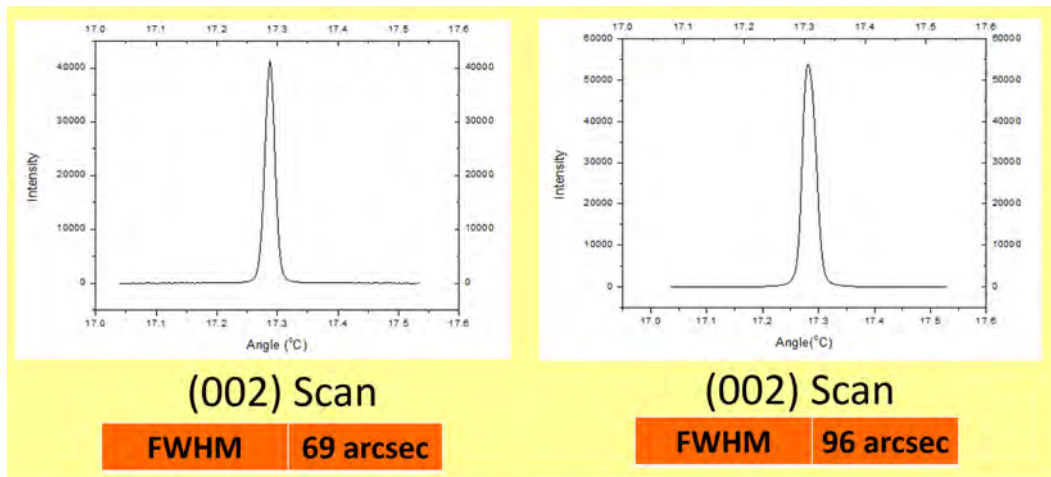


Figure 5.4: Left: Sample G007, Right: Sample G008

(c) Off-axis x-ray rocking curve value ³

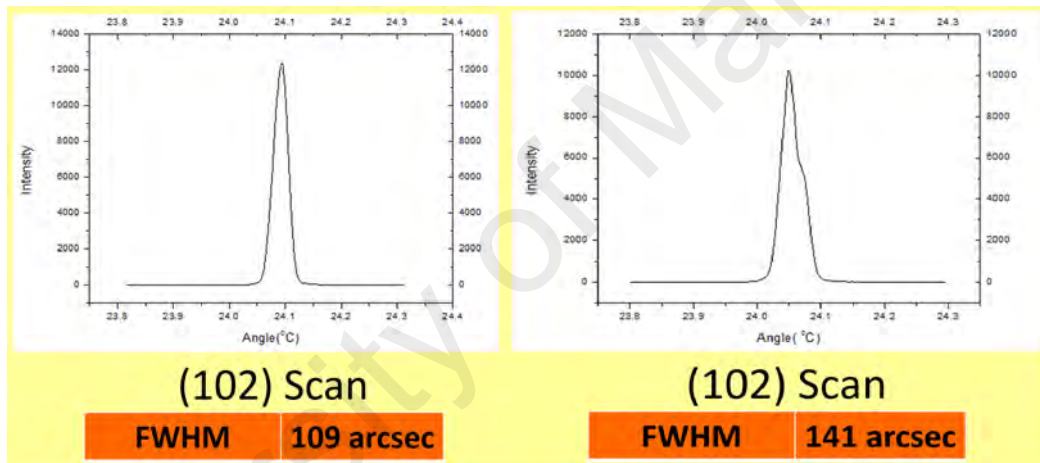


Figure 5.5: Left: Sample G007, Right: Sample G008

Table 5.2 explains the dislocation density of 002 and 102 plan as well as the total dislocation densities for sample G007 and G008. Each dislocation density was obtained from the arcsec value. The arcsec unit was converted to degree (radian) and using Equations 5.1 or 5.2 . Take note burger vector b_{screw} and b_{edge} were in nm unit. To obtain the dislocation density in cm^{-2} unit, the burger vector changed to cm unit during initial calculation. The total dislocation density obtained from the calculation of sample G007 and G008 is $3.51 \times 10^7 \text{ cm}^{-2}$ and 6.00×10^7

³ (102) scan taken from Uid-GaN

Table 5.2: XRC-FWHM of the 002 and 102 plan and the screw N_{screw} and edge N_{edge} dislocation densities for G007 and G008

Sample no.	FWHM of XRC, arcsec		$N_{\text{screw}}, \text{cm}^{-2}$	$N_{\text{edge}}, \text{cm}^{-2}$	$N_{\text{total}}, \text{cm}^{-2}$
	Scan (002)	Scan (102)			
G007	69	109	4.63×10^6	3.05×10^7	3.51×10^7
G008	96	141	8.96×10^6	5.11×10^7	6.00×10^7

cm^{-2} respectively. Since these samples from same GaN substrates which has the dislocation density at $4.10 \times 10^6 \text{ cm}^{-2}$. Hence the dislocation density increased by order of one on undoped GaN. This prove that undoped GaN has high quality GaN layer on bulk GaN substrates.

(d) RMS roughness as measured by AFM

The root mean square, RMS of roughness qualitatively explain the surface smoothness. The bigger the RMS value the more rougher the epitaxial grown surface is. For sample G007 the RMS roughness of 0.48 nm. From literature the rms roughnesses of 0.49 and 0.31 nm for m-plane and c-plane substrates, respectively (Lai et al., 2009). This shows a flat surface of undoped GaN and ready for active layer (MQWs) to be grown. ⁴

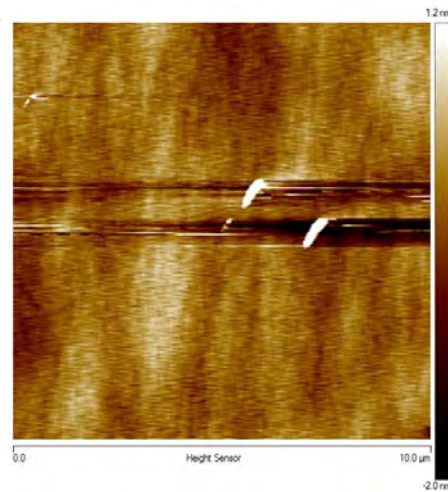


Figure 5.6: RMS of surface roughness on Uid-GaN, Sample G007 at 0.48 nm

⁴ The two white spots (contamination) were ignored during RMS calculation.

(e) Silicon concentration

Referred to Table 1.1, the silicon concentration target should be at least 5.0×10^{18} atom/cm³. In addition to this there are parameters such as carrier mobility, resistivity and RMS roughness targets used as optimization measure of n-GaN layer. All mentioned target closely related to each other whether altered the physical or electrical or both properties when certain amount of dopant introduced into epitaxial GaN layer while growth. Targeting a desired silicon concentration value in the crystal the silane flow rate or flux need to be changed. Samples G074 and G075 the silane flux at 35 and 45 sccm respectively.

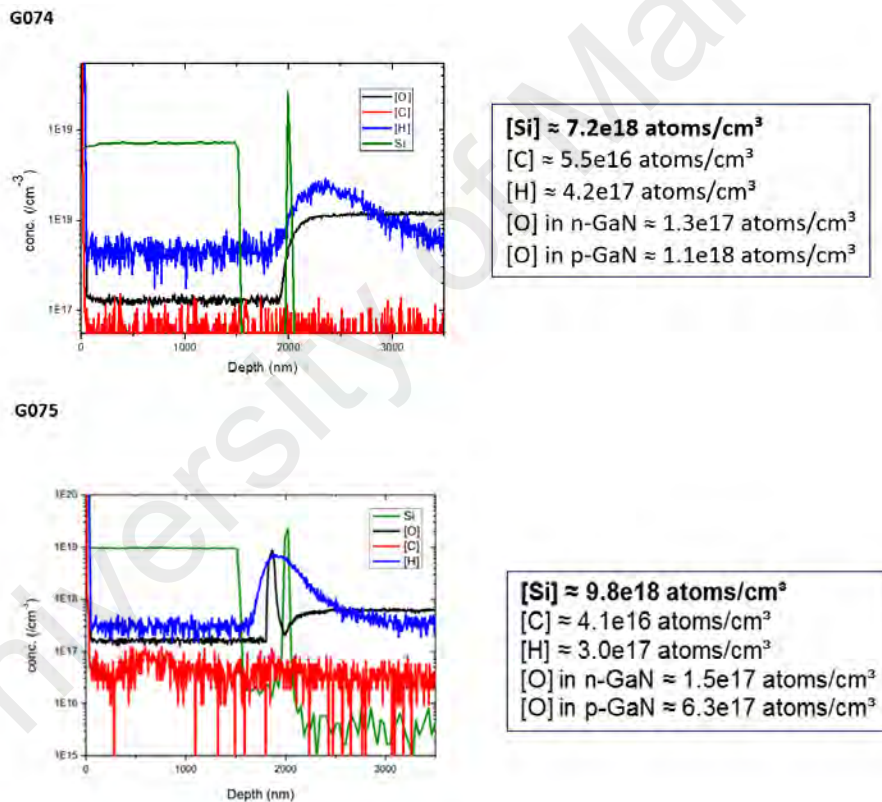


Figure 5.7: [Si], Top: Sample G074, Bottom: Sample G075

Using SIMS analysis the silicon concentration obtained for samples G074 and G075 of 7.2×10^{18} atom/cm³ and 9.8×10^{18} atom/cm³ respectively shown on Figure 5.7 and simple Table 5.3. The more the silane flux used the higher the silicon concentration (only for certain range). Always need to ensure the

background oxygen concentration content at order of 17 or lesser. Or else the oxygen will contribute to n-type (n-GaN) and even change the nature of p-type (p-GaN) layer to more to n-type.

Table 5.3: n-GaN Silicon concentration

Sample no.	Silicon concentration, atom/cm ³
G074	7.2×10^{18}
G075	9.8×10^{18}

(f) Mobility

In solid-state physics, the carrier mobility characterizes how quickly a positive or negative carrier can move in semiconductor material, in presence of electric field. For LED mobility it is very important parameter that reveals the quality of the crystal and how efficient the LED device will perform. The mobility doesn't only depend on amount of dopant introduced also it is depend on the quality of the crystal (defects). The recorded mobility for samples G074 and G075 using Hall measurement of 271 and 269 cm²/Vsec respectively shown in Appendix B. Mobility of G074 is higher compared to G075.

(g) Resistivity

Electrical resistivity is the fundamental property that quantifies how strongly a given material opposes the flow of current. Conductivity, σ is defined as the inverse of resistivity, ρ . Hence the Equation 5.3 transformed to Equation 5.4. From that carrier concentration has taken as the subject and formed Equation 5.5. However the result from Hall measurement from Figure 5.8 most of it in sheet resistivity, sheet coefficient and sheet carrier density. Where n , e , μ_e , ρ_{\square} , t , n_{\square} are called carrier concentration, charge of an electron, mobility of electron, sheet resistivity, epitaxial thicknesses and sheet carrier concentration respectively. The electron carrier concentration calculated using two ways that were using

Equations 5.5 and 5.7. The electron carrier concentration, n related to sheet carrier concentration of electron n_s equation 5.6. Using data on Appendix B for sample no. G074, where $t = 1.5 \times 10^{-4}$ cm (from Table 5.1), the resistivity, $\rho = 3.3 \times 10^{-5}$ $\Omega \cdot \text{cm}$ (from Table 5.4). From Equation 5.5, the electron carrier concentration, $n = 7.0 \times 10^{20}$ cm^{-3} . From Equation 5.7, electron carrier concentration, $n = 7.0 \times 10^{20}$ cm^{-3} . Both method show same value of n , due to each parameter from Figure 5.8 interrelated.

$$\sigma = ne\mu_e \quad (5.3)$$

$$1/\rho = ne\mu_e \quad (5.4)$$

$$n = 1/\rho e\mu_e \quad (5.5)$$

$$\rho = \rho_{\square} t \quad (5.6)$$

$$n = n_{\square}/t \quad (5.7)$$

Compared to electron carrier concentration, n (7.0×10^{20} cm^{-3}) and silicon concentration (7.2×10^{18} cm^{-3}) should be the same if the each silicon atom ionized to release an electron. However it is not the same. Highly suspect due to the impurity in the crystal such oxygen and etc might contributed into increment by order of 2 compared to silicon concentration.

Table 5.4: n-GaN sheet resistivity and resistivity

Device no.	Sheet Resistivity, Ω/\square	Resistivity, $\Omega \cdot \text{cm}$
G074	0.22	3.3×10^{-5}
G075	0.21	3.3×10^{-5}

(h) RMS roughness

The RMS roughness for samples G074 and G075 of 0.4 nm and 0.9 nm have respectively shown in Figure 5.8. This clearly shows that, the high silicon dopant concentration altered the properties of the epitaxial crystal layer made more rougher. Overall the G074 with silane 35 sccm was the best in term of morphological and electrically.

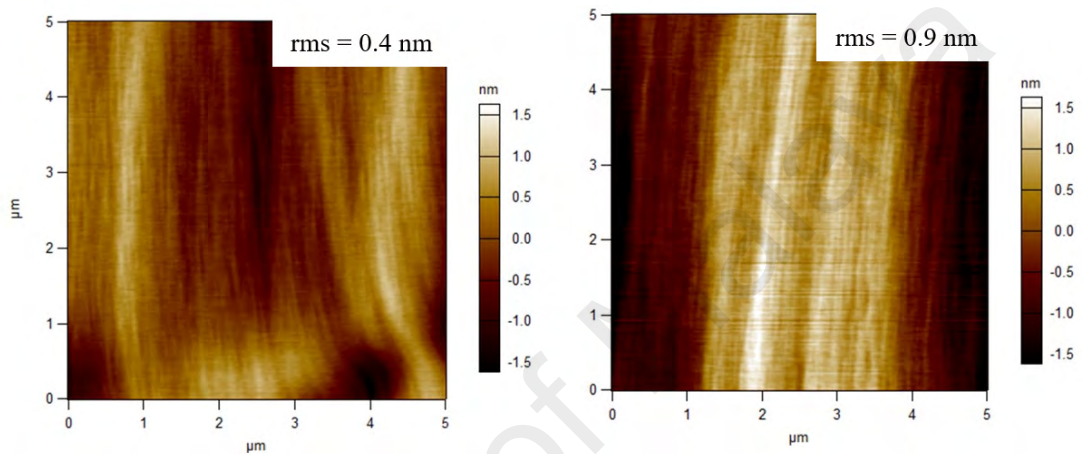


Figure 5.8: Surface roughness, Left: Sample G074, Right: Sample G075

(i) Blue light emission from CL

The wavelength light emission from active layer (MQWs) determined by CL, EL or PL. Here PL was used. Referred Figure 5.9 and Table 5.5 the samples G046 and G073 the blue light emission of 446 nm and 451 nm respectively.

Table 5.5: MQW Blue light emission met the targeted range of 455 nm \pm 10 nm

Sample no.	MQW Blue light emission, nm
G046	446
G073	451

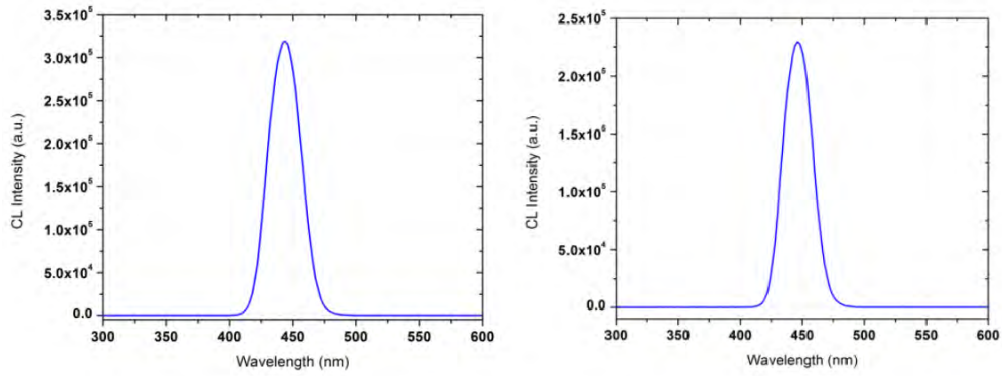


Figure 5.9: CL spectrum, Left: Sample G046, Right: Sample G073

(j) Mg concentration

Generally atom silicon used a dopant onto GaN layer to formed n-GaN, same as atom magnesium, Mg doped onto GaN to formed p-GaN. The magnesium source form Cp2mg precursor. Not every atom magnesium releases a hole. In addition the background impurity effects the hole concentration. Due to this the magnesium concentration should be targeted higher compared to silicon concentration. The Cp2mg precursor flow adjusted at a rate 35 sccm and 20 sccm for G060₁ and G060₂ respectively. SIMS was used to analyze the magnesium concentration and found 5.0×10^{19} atom/cm³ and 2.2×10^{19} atom/cm³ for samples G060₁ and G060₂ respectively shown in Figure 4.1 and the summary in Table 5.6.

Table 5.6: SIMS result, refer to Figure 4.1 for G060₁ at 35 sccm and G060₂ at 20 sccm

Sample no.	Mg concentration, atom/cm ³
G060 ₁	5.0×10^{19}
G060 ₂	2.2×10^{19}

(k) L-I-V result

G073 is called as device no. instead of sample no., since it is a full growth LED. Figure 5.10 two graphs plotted on the same axis. The vertical left axis is light output power, LOP/W and vertical right axis (blue) is voltage, V/V vs current applied, I/mA. At different current supply the LOP and V responds differently. Take note as the current increases the P rate of increment slows down (called droop effect). Usually the standard practice to measure the P and V at 20 mA per unit area (cm^2)(current density). At current density at 20 A/cm^2 the LOP at 2.0 mW and V at 4.5V shown Table 5.7.

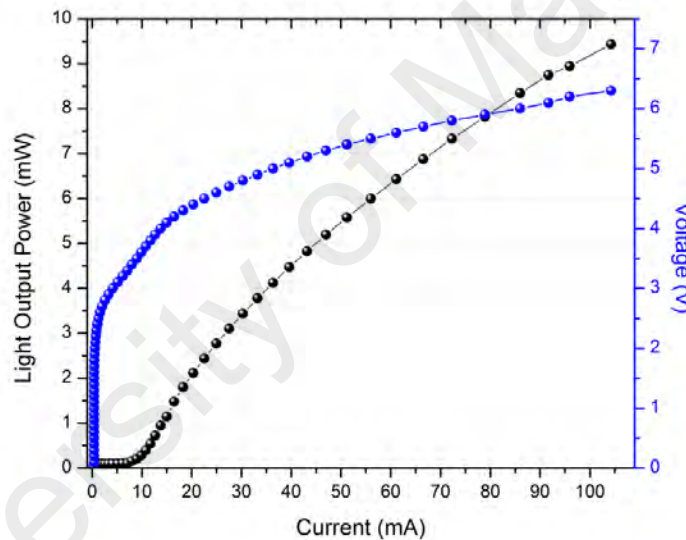


Figure 5.10: Light output power and voltage vs current

Table 5.7: L-I-V result

Device no.	V _f (V) @ 20 A/cm ²	LOP (mW)@ 20 A/cm ²
G072	4.5	2.0

(l) Spectrum result

The EL measurement for intensity vs the wavelength spectrum plotted shown on Figure 5.11. The peak wavelength of 448 nm and FWHM of 21 nm at 20 A/cm^2 . The smaller the FWHM value the narrower the spectrum will be. Narrowed

spectrum explain the high quality LED crystal layer especially the active layer (MQWs).

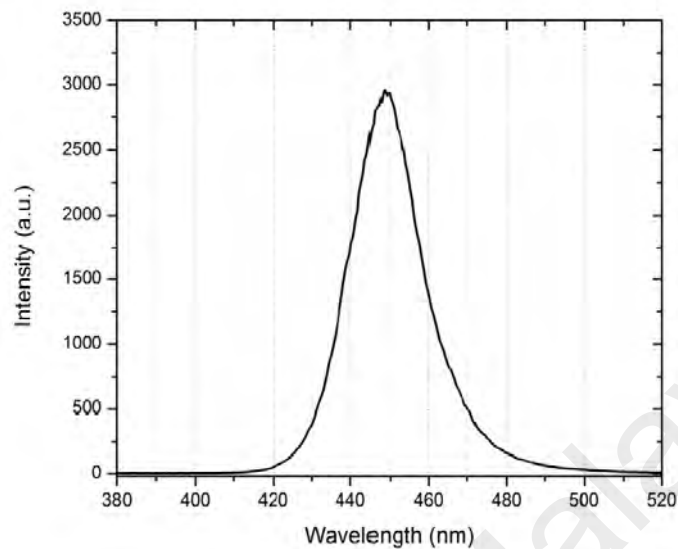


Figure 5.11: EL wavelength spectrum

5.3 Summary

Growth and optimization of GaN-on-GaN LED firstly started with undoped GaN getting the right growth rate without jeopardizing the crystal quality at same time where the omega scan (arcsec) and RMS surface roughness parameter controls that. Once the growth rate obtained. The growth of n-GaN on bulk GaN was proceeded. The silane flux adjusted to accommodate the silicon concentration, mobility, resistivity and RMS roughness targets. After n-GaN optimized, the active layer InGaN/GaN multi-quantum wells were stack on n-GaN (thicknesses of 1-2 μm). The indium contents in the quantum wells (QWs) of $\text{In}_x\text{Ga}_{1-x}\text{N}$ alloys varies with temperature. The indium content of the quantum wells controlled by the growth temperature. The desired blue emission were obtained on G073 at 685 $^\circ\text{C}$ for both QWs and QBs inclusion of p-GaN layer. The optical properties such as peak wavelength at 448 nm and FWHM at 21 nm. The electrical properties LOP at 2.0 W and voltage recorded at 4.5 V at 20 A/cm^2 current supply.

CHAPTER 6: RESULTS AND DISCUSSION: DEMONSTRATION OF FIRST GaN-ON-GaN BLUE LED IN MALAYSIA

6.1 Introduction

Malaysia is the important player in electronic world. Due to the high demand in LEDs market pushes us into optoelectronic as well. UM, and CREST collaboration with other major industries such OSRAM have provided a platform and creating LEDs awareness in Malaysia. UCSB technology transfer and guidance have given LMDRC, UM Malaysia to demonstrate the first GaN-on-GaN LED in Malaysia.

6.2 First GaN-on-GaN Blue LED

This section is divided into 2 parts. The first parts the blue GaN-on-GaN LEDs partially grown in Malaysia and UCSB. Followed by the second part blue GaN-on-GaN LEDs fully grown in Malaysia. The partial growth LED due to inline purifier saturated. Hence the p-GaN was grown at UCSB to fasten the demonstration process. Figure 6.1 shown LED section grown at Malaysia and UCSB. Note: Figure 5.1 is the standard LED structure, however only here the first GaN-on-GaN blue LED demonstrated.

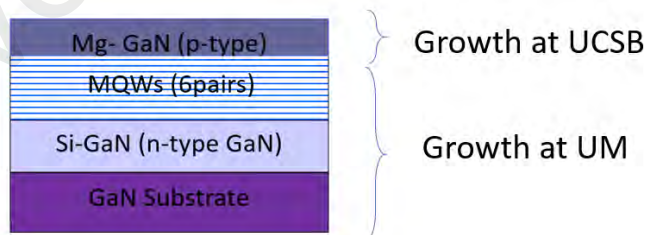


Figure 6.1: Blue GaN-on-GaN LEDs partially grown in Malaysia and UCSB

After the active region completed, the growth was aborted at this step. Then the sample G048 sent to UCSB for p-GaN regrowth. Before growth the sample was cleaned using: Acetone for 15 mins, isopropyl alcohol (ISO) for 15 mins, UV ozone for 15 mins and HF

dip for 1 min. This process was repeated for 3 times. The sample grew for allowing steps p-GaN and p⁺-GaN for 20 mins and 2 mins, respectively. For steps p-GaN the flow rates at NH₃, TEG and Cp2Mg are 0.223 μmol/min, 5.52 μmol/min and 5.7 sccm for p-GaN, respectively. The flow rates at NH₃, TEG and Cp2Mg are 0.268 μmol/min, 8.05 μmol/min and 26 sccm for p⁺-GaN, respectively.

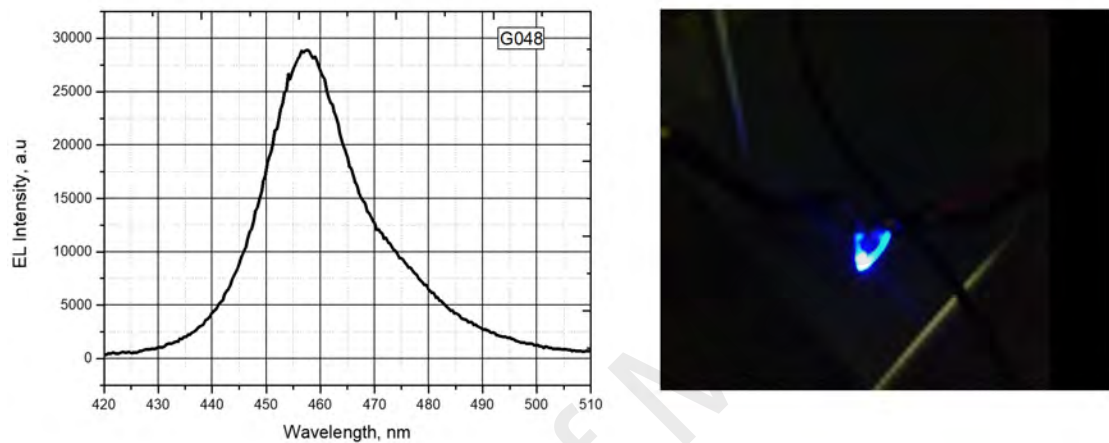


Figure 6.2: Blue GaN-on-GaN LEDs partially grown in Malaysia and UCSB: EL spectrum

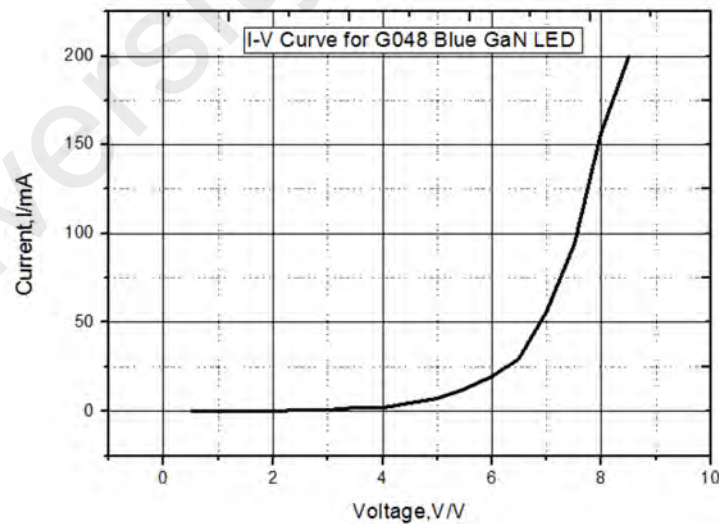


Figure 6.3: Blue GaN-on-GaN LEDs partially grown in Malaysia and UCSB, I-V curve

By applying current of 20 mA, the voltage observed is 5.88V and power is 0.035 mW. The peak wavelength of 458 nm and FWHM of 20 nm. The second part fully grown at UM, Malaysia. Compare to first part the gallium MO source was TMG, however the second part using TEG as a gallium MO source. The TEG has better contamination quality control from carbon during MQWs or active region growth. In addition the MOCVD using inline and regeneration purifier for ultra-high purity for better MQWs quality. The estimated MQWs thickness for QW and QB is 2.8 nm and 14 nm, respectively.

Table 6.1: Blue GaN-on-GaN LEDs fully grown in Malaysia

Device no.	EL, QT result @ 20 mA	Active region temperature, T/°C
G072	λ : 429 nm, Power: 1.3 mW	695
G073	λ : 444 nm , Power: 1.0 mW	685

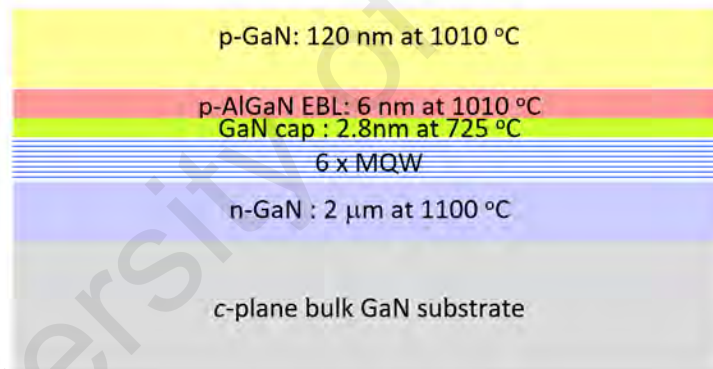


Figure 6.4: Blue GaN-on-GaN LEDs fully grown in Malaysia for device no. G072 and G073

Referred to Figure 6.5 and Table 6.1 show the peak wavelength recorded for samples G072 and G073 of 429 nm and 444 nm, respectively. G073 peak wavelength increased by 15 nm compared to peak wavelength of G072. The growth temperature of active layer (MQWs) at 695 °C and 685 °C, respectively. The higher the MQWs growth temperature the higher the desorption rate of indium from MQWs layer. The less contain of indium causes the peak wavelength emission shifted to shorter wavelength (blue shift).

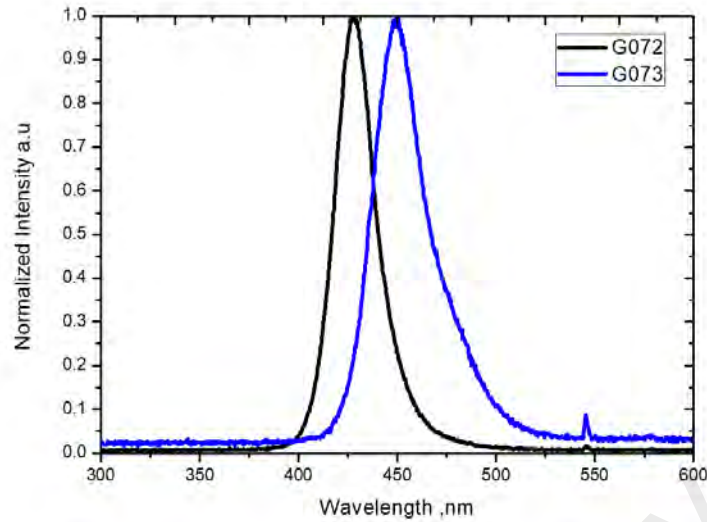


Figure 6.5: EL spectrum for device no. G072 and G073 of blue GaN-on-GaN LEDs fully grown in Malaysia

Table 6.2: Blue GaN-on-GaN LEDs fully grown in Malaysia for device no. G072 and G073

Device no.	FWHM, nm
G072	24
G073	32

Referred to Table 6.1 and 6.2 the FWHM value larger from EL and power lower from quick test, QT for G073 compared to G072. This highly suspect due to the MQW growth temperature was too low and resulting a poor crystal quality of MQWs (active layer).

6.3 Summary

The first blue LED grown partially and fully grown shows a power of 0.035 mW and 1.0 mW on sample G048 and G072, respectively. Using triethylgallium (TEG) for MQWs growth as gallium source always a better choice in rate growth control and less carbon contamination instead of TMG. GaN-on-GaN blue LEDs in Malaysia successfully demonstrated. This is a great start and to show potential in optoelectronic research field and as the technology provider locally.

CHAPTER 7: RESULTS AND DISCUSSION: NOVEL FINDINGS; EFFECT OF THERMAL INTERACTION BETWEEN BULK GAN SUBSTRATES AND CORRAL SAPPHIRE

7.1 Introduction

This study demonstrates that there is difference growth conditions during multi-quantum wells growth on bulk GaN substrates and surrounded by the sapphire corral referred to Figure 3.3. The InGaN/GaN multi-quantum wells were grown on bulk GaN substrate. The indium contents in the quantum wells (QWs) of $\text{In}_x\text{Ga}_{1-x}\text{N}$ alloys varies with temperature and desorbed at high temperatures. However, too low temperatures growth will affect the crystalline quality of the grown material. Generally, less indium content of the quantum wells will lead to blueshift. The heat interaction of these materials towards the heat source is due to their intrinsic thermodynamic properties. The results indicate that the magnitude of deviation in heat interaction is largely determined by the thermal conductivity properties of these two materials (GaN and sapphire). The differences in heat interaction shows shift in peak wavelength from the desired target value. To measure the peak wavelength emission of multi-quantum wells, photoluminescence was employed and a computational method was used for in-depth understanding of the heat interaction.

7.2 Observation

By referring to Table 7.1 and Figure 7.1, the GaN cap thickness used for higher temperature barrier, HT-Barrier MQWs on sapphire wafer at 1.2 nm for sample A. Sample B was subjected to the similar condition as sample A but at different growth temperature. The QW growth condition applied on sample A and sample B were 716 °C and 703 °C with the corresponding peak wavelength of 463 nm and 433 nm for sample A and sample B respectively. The grown of sample B at lower temperature does not show any increase in wavelength but instead it shows a shorter wavelength. Furthermore, analysis done on the

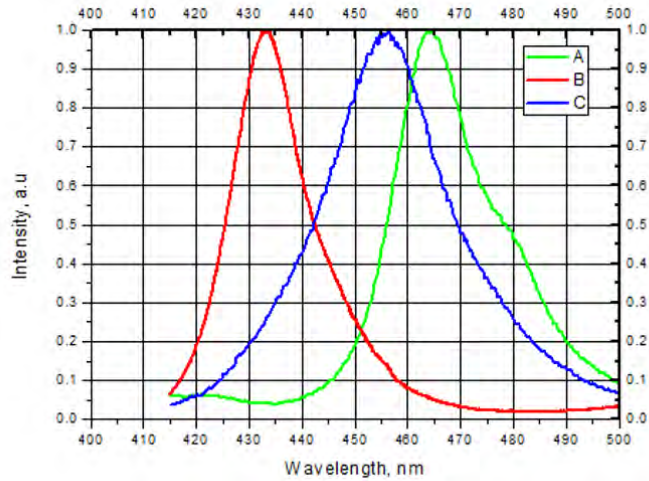


Figure 7.1: Sample A, B, and C's wavelength spectrum from PL

Table 7.1: Sample A grown on whole sapphire, sample B and C on bulk GaN substrates with sapphire corral

Sample	Substrates	GaN cap	Temp, °C		Peak wavelength, nm
			QW	QB	
A	Sapphire	25	716	777	463
B	Sapphire	25	703	777	433
C	GaN-Sapphire	25	697	697	455

low-temperature barrier at 697 °C and applied to sample C. The peak wavelength nearer to the target wavelength differs only by 5 °C from target value. To target MQWs wavelength at 450 nm on bulk GaN high temperature barrier growth it is a great challenge as compared to sapphire. This shows the condition applied during MQWs growth based on sapphire and bulk GaN were different.

Similar observations were quoted in other journals, summarized in Table 7.2. In reference (Young et al., 2013) for #1 and #2 shows similar plane applied (c-plane) yet the QWs thicknesses are not the same (note: materials were different). If different substrate material and crystal plane were to used, a thicker QW layer and lesser indium composition on m-plane (#4) were observed compared to sapphire sample (#3) (Lai et al., 2012). If substrate used from same material even different crystal orientation employed the m-plane (#5) and c-plane GaN (#6) exhibits similar QW thickness and indium percentage (Lai et

Table 7.2: Summary of previous research on growth with different substrates

#	Substrates	Temperature /°C	Indium composition /%	QW thickness /nm	CL /nm	EL /nm
1	Sapphire	at same temperature	-	2.3	-	-
2	c-plane GaN		-	3	-	-
3	Sapphire	750	13.9	1.7	460	-
4	m-plane GaN		5.1	4.4	397	-
5	c-plane GaN	750	5.4	same thicknesses	416.5	-
6	m-plane GaN		5.3		397	-
7	Sapphire	890	-	-	-	450-460
8	m-plane GaN	875	-	-	-	400-410

al., 2009). The argument is if due to quantum-confined Stark effect (QCSE) during CL measurement on the c-polar and non-polar the peak wavelength different is significant between (#3) and (#4) compared to (#5) and (#6). The reference (Kim et al., 2007) displays the growth temperature of QW around 890 °C and the 450–460 nm peak wavelength on c-plane sapphire (#7), however at 400–410 nm peak wavelength was achieved at 875 °C on m-plane bulk GaN (#8) substrates matches the similar report in this paper. These narrows down to a conclusion that substrates selection plays a major role in peak wavelength shift compared to strain layers, QCSE, crystal orientation etc.

Furthermore, analysis done on the low-temperature barrier at 697 °C and applied to sample B. The peak wavelength nearer to the target wavelength differs only by 5 °C. By taking the similar temperature of QB and QW with keeping 1.2 nm GaN cap thickness, the 455 nm wavelength was established on sample C. To target MQWs wavelength at 450 nm on bulk GaN high temperature barrier growth it is a challenge if compared to sapphire. This shows the condition applied during MQWs growth based on sapphire and bulk GaN were different.

7.3 Analysis using simulation method by COMSOL

An enclosed chamber with temperature-controlled walls with a set point of 293.15 K. The geometry of the chamber walls can be omitted since it is in a closed cavity. Furthermore, the model assumes that this physical system is dominated by radiation and convection cooling (Roozeboom, 2013; Borisenko & Hesketh, 2013). The convective cooling of the wafer to the gas (at 453.15 K) is modelled by using a heat transfer coefficient, h (in this model set to 29.5 W/m²K). The temperature uniformity is mainly achieved through specific Lamp configuration design (Fukuda, 2003; Jan & Lin, 1998) and since that was not the focus of our study, thus using wider surface heat source is sufficient.

$$\rho C_p \frac{\partial T}{\partial t} + \Delta \cdot (-k \Delta T) = Q \quad (7.1)$$

$$-n \cdot (-k \Delta T) = h(T_{inf} - T) + \frac{\epsilon}{(1 - \epsilon)} (J_0 - \sigma T^4) \quad (7.2)$$

The problem is governed by the heat equation shown 7.1, given below together with its boundary condition shown 7.2 (Fukuda, 2003) which is solved using the existing heat transfer module in the commercial software COMSOL Multiphysics (Comsol, 2018; Pryor, 2009). Where ρ is the density, k denotes the thermal conductivity, Q represents the volume heat source, n is the surface normal vector, T_{inf} equals the temperature of the convection cooling gas, denotes the surface emissivity, is the expression for surface radiosity and is the Stefan-Boltzmann constant. The interval between heating and stable stage is the QB condition and cooling to the stable stage is the QW condition shown in Figure 7.2

To understand the growth condition, the nature of the material used of substrates and corral need to be verified. Table 7.3 shows the parameters for each material as GaN, sapphire, and silicon. Therefore, thermal conductivity is important parameters in predicting the thermal energy transfer through materials. The value of specific heat capacity, C_p at

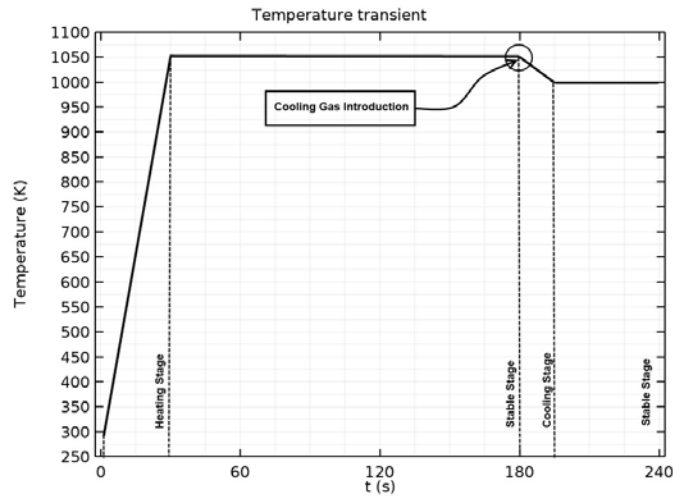


Figure 7.2: Rapid thermal processing plan used in this model

Table 7.3: GaN and sapphire constants

Material	Density, g/cm ³ at r.t.p	Thermal conductivity, K W/mK at r.t.p	Specific heat capacity, C _p Jkg ⁻¹ K ⁻¹ at 697 °C	Ratio of Thermal conductivity
GaN	6.15	253	624	GaN: sapphire=8:1
Sapphire	3.96	30.3	1220	-

697 °C calculated from the temperature-dependent equation, refer to (Lee et al., 2011; Dobrovinskaya et al., 2009; Endo et al., 2003) for GaN, sapphire and silicon material, respectively. Thermal conductivity and density assumed constant at room temperature pressure, r.t.p. All constants inputted in COSMOL simulation purpose (Shibata et al., 2007; Jin et al., 2014).

The key interests are the ratio of thermal conductivity value. The ratio of thermal conductivity of GaN: sapphire is 8:1. This shows the tendency of heat transfer to GaN material is relatively higher compared to sapphire material from heat source. Heat interaction studies between two different materials were done by using the simulation method to predict the surface temperature differences between bulk GaN and corral sapphire. Thus, the PL emission of InGaN/GaN MQWs on based bulk GaN at high-temperature barrier growth was checked. Figure 7.3 shows the modeling result using COMSOL for

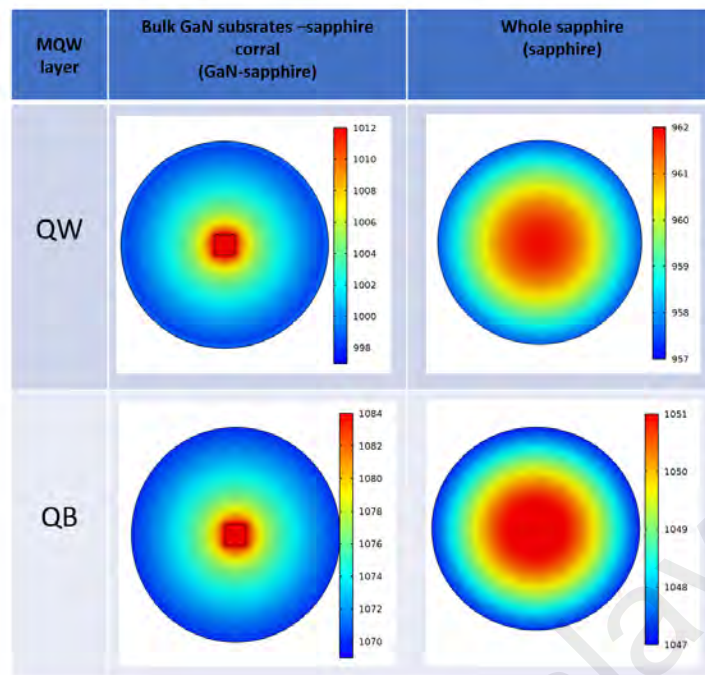


Figure 7.3: Wafer temperature profile of GaN-sapphire and sapphire from COS-MOL simulation

QW and QB at 697 °C and 777 °C, respectively.

Since the corral covered most of the area 2 inches, the possibility of the thermocouple takes the corral temperature reading as compared to GaN is high. The heater will continually supply a constant thermal rate to the wafer to achieve the setting temperature value given based on corral. Subsequently, that amount of heat enough to raise the GaN temperature about 10 °C compared to corral sapphire due to thermal conductivity ratio of 8:1 compared to sapphire material. The table 7.4 shows further analysis on temperature variation in the whole sapphire, silicon and GaN at 5 °C and 1 °C respectively. This shows the variation is high on the whole sapphire if compared to whole GaN. If LEDs grown on whole GaN substrates, the total wavelength variation within wafer will be lesser compared to sapphire. The homogeneous epitaxy of GaN-on-GaN produces the unprecedented epitaxy crystal quality and performance LED. Furthermore, GaN substrates would give less total wavelength variation within a single wafer and subsequently better reproducibility LED chips from a single wafer. Referred to Figure 7.3 the simulation was done at 697 °C and

Table 7.4: Maximum temperature difference in the wafer for different substrate types from the COSMOL simulation

MQW layer	MQW Temperature, °C	Total temperature variation by substrates type, °C		
		GaN-Sapphire	Sapphire	GaN
QW	697	15.0	5.0	1.0
QB	777	15.0	4.0	1.0

777 °C respect to QB and QB condition. Taking the area of interest at wafer centre their respective temperatures from Figure 7.3 was constructed to Table 7.5. The temperature difference between targeted and obtained, which simulation were -8 and +42 on sapphire and GaN-sapphire, respectively for QW layer. Whereas the temperature difference were 0 and +34 for sapphire and GaN-sapphire, respectively for QB layer. This significantly prove the effect of substrates selection as it with corral or without. The thermal conductivity gap of GaN and sapphire material has raise to larger temperature deviation compared to sapphire substrates.

Table 7.5: Simulated temperature of MQW

MQW layer	Substrates	Temperature T/°C		
		Targeted	Obtained	Difference
QW	Sapphire	697	689	-8
	GaN-sapphire	697	739	+42
QB	Sapphire	777	777	0
	GaN-sapphire	777	811	+34

From the temperature difference value from Table 7.5 a re-corrected MQWs temperature was calculated shown in Table 7.6. Based on sample A, the sapphire substrates was employed and actual QW growth temperature of 708 °C was grown cooler than expected corresponded to a peak wavelength at 463 nm. Whereas the sample B the QW growth temperature targeted at 703 however grew at very high temperature about 745 °C and corresponded peak wavelength at 433 nm(blue shift). Furthermore, for sample C was grown at 697 °C and the expected QW temperature of 739 °C which is lower compared to sample B. Although the QB temperature contributed into peak wavelength shift, however

the right QW growth temperature with optimized GaN-cap thicknesses will ensure better process control toward the indium desorption and overall maintaining the peak wavelength. Compared to sample A and B their growth set temperature peak wavelength has not rational. However with re-corrected MQW temperature it is possible. This clearly justified the hypothesis of the substrates selection is a factor.

Table 7.6: Re-corrected MQW temperature

Sample	Substrates	Temp, °C		Re-corrected temp, °C		Peak wavelength, nm
		QW	QB	QW	QB	
A	Sapphire	716	777	708	777	463
B	GaN-Sapphire	703	777	745	811	433
C	GaN-Sapphire	697	697	739	739	455

7.4 Summary

This study demonstrated the surface temperature of bulk GaN substrate is higher about 10 °C-15 °C compared to corral sapphire based the thermal conductivity and not considering the surface roughness. This proved that the growth condition on GaN-sapphire and whole GaN substrate are different, 42 °C needed to be compensated while growing LEDs on whole bulk GaN substrates to achieve the desired wavelength. Growth of LED on bulk GaN using low-temperature barrier will be better process control option. In comparison, the whole bulk GaN substrate will have better light emission uniformity across wafer compare to sapphire material provided similar MQWs layers applied. In brief, the growth with or without corral, usage of corral type, size of bulk GaN substrate may caused temperature change on c-plane bulk GaN substrate and corral. The difference in growth rate of MQWs and percentage of indium content subsequently leads to a difference in PL, CL or EL emission due to the thermal interaction between conditions mentioned.

CHAPTER 8: CONCLUSION AND SUGGESTIONS

The work of this dissertation has covered an experimental efforts to produce GaN-on-GaN blue LEDs first in Malaysia. Whether this work can be described as ground-breaking or not, it is built upon a foundation of work which has been painstakingly built up over the course of decades of research by hundreds of scientists. This research is important to establish the next-generation high-efficiency blue and white light emission LED for lighting application. The effort taken by Malaysian government should be appreciated. The optoelectronic ecosystem provided by Malaysia created a work platform with renowned industry like OSRAM and international research team such as UCSB. Processing a single takes 2-5 hours and cost per hour about RM1000. MOCVD growth research is very expensive research. Due to this it limits the research in way such as repetitive growth it a great challenge. This reduces the repeatability study and uncertain on precision of a measurement. Furthermore, the peak wavelength emission sensitive to small distribution such as reactor temperature shift, dirty flow channel, saturated inline purifier, byproduct inside reactor and etc. The metrology tools are limited in UM. It is very essential to have tools such as SIMS, HDXRD, CL, TEM and more in UM. This delay the interpreting data and the overall project time-line. The direction of GaN-on-GaN project was very clear with 12 key parameters to achieve provided by the UCSB and Crest board of members. Technically the introduction of HT-barrier technique found better improvement compared to insertion of SLS at 92% and 60% on defect density and RMS surface roughness, respectively. The demonstration of first GaN-on-GaN blue LED in Malaysia on G073 at 448 nm LOP at 2.0 W, voltage recorded at 4.5 V at 20 A/cm². Finally the novel finding, the growth with or without corral, usage of corral type, size of bulk GaN substrate may caused temperature change on c-plane bulk GaN substrate and corral. Since it a great

start in solid state LED research and development in Malaysia there are plenty room for learning and improvement. Since the MQWs (active region) is the most important layer, the defect analysis on this area is essential. By using N_2/H_2 mix gases as carrier during QB growth could help to improve by reducing the V-pit in MQWs structure. Using the non-polar bulk GaN substrate is the best to eliminate the polarization effect for higher efficient and brighter LEDs. Proper choices of a suitable bulk GaN substrate is vital by considering on the dislocation density and FWHM value to ensure high quality substrate crystal being used.

University of Malaysia

REFERENCES

- Akasaki, I., Amano, H., & Nakamura, S. (2014). Blue LEDs-filling the world with new light. *Nobel Prize Lecture*.
- Armstrong, A., Kelchner, K., Nakamura, S., DenBaars, S., & Speck, J. S. (2013). Influence of growth temperature and temperature ramps on deep level defect incorporation in m-plane GaN. *Applied Physics Letters*, *103*(23), 232108.
- Ayers, J., Kujofsa, T., Rago, P., & Raphael, J. (2016). *Heteroepitaxy of semiconductors: Theory, growth, and characterization, second edition*. CRC Press.
- Bayo, C. (2013). *Theory of elasticity and electric polarization effects in the group-III nitrides*. Retrieved on 28 February 2017, <https://cora.ucc.ie/handle/10468/1344>.
- Becerra, D. L., Zhao, Y., Oh, S. H., Pynn, C. D., Fujito, K., DenBaars, S. P., & Nakamura, S. (2014). High-power low-droop violet semipolar (3031) InGa_N/Ga_N light-emitting diodes with thick active layer design. *Applied Physics Letters*, *105*(17), 171106.
- Borisenko, V., & Hesketh, P. (2013). *Rapid thermal processing of semiconductors*. Springer United States of America.
- Brodusch, N., Demers, H., & Gauvin, R. (2017). *Field emission scanning electron microscopy: New perspectives for materials characterization*. Springer Singapore.
- Carter, C., & Norton, M. (2007). *Ceramic materials: Science and engineering*. Springer New York.
- Chang, S.-J., Lai, W.-C., Su, Y.-K., Chen, J.-F., Liu, C.-H., & Liaw, U. (2002). InGa_N-Ga_N multiquantum-well blue and green light-emitting diodes. *IEEE Journal of Selected Topics in Quantum Electronics*, *8*(2), 278–283.
- Chen, C., Gaevski, M., Sun, W., Kuokstis, E., Zhang, J., Fareed, R., . . . others (2002). Ga_N homoepitaxy on freestanding (1100) oriented Ga_N substrates. *Applied Physics Letters*, *81*(17), 3194–3196.
- Choi, Y.-S., Park, J.-H., Kim, S.-S., Song, H.-J., Lee, S.-H., Jung, J.-J., & Lee, B.-T. (2004). Effects of dislocations on the luminescence of Ga_N/InGa_N multi-quantum-well light-emitting-diode layers. *Materials Letters*, *58*(21), 2614–2617.
- Comsol. (2018). *Comsol*. Retrieved on 2 March 2017, <http://www.comsol.com>.

- Copel, M., Reuter, M., Kaxiras, E., & Tromp, R. (1989). Surfactants in epitaxial growth. *Physical Review Letters*, 63(6), 632.
- Dobrovinskaya, E. R., Lytvynov, L. A., & Pishchik, V. (2009). *Sapphire: Material, manufacturing, applications*. Springer.
- Endo, R. K., Fujihara, Y., & Susa, M. (2003). Calculation of the density and heat capacity of silicon by molecular dynamics simulation. *High Temperature - High Press*, 35(36), 505–511.
- Evans, M., Glueckstein, J., & Nogami, J. (1996). Epitaxial growth of manganese on silicon: Volmer-weber growth on the Si (111) surface. *Physical Review B*, 53(7), 4000.
- Feezell, D., & Nakamura, S. (2018). Invention, development, and status of the blue light-emitting diode, the enabler of solid-state lighting. *Comptes Rendus Physique*.
- Fukuda, H. (2003). *Rapid thermal processing for future semiconductor devices*. Elsevier.
- Gayral, B. (2017). LEDs for lighting: Basic physics and prospects for energy savings. *Comptes Rendus Physique*, 18(7-8), 453–461.
- Gil, B. (2014). *Physics of wurtzite nitrides and oxides: Passport to devices*. Springer International Publishing.
- Gupta, K., Gupta, N., & Tiwari, A. (2015). *Advanced electrical and electronics materials: Processes and applications*. Wiley.
- Haugstad, G. (2012). *Atomic force microscopy: Understanding basic modes and advanced applications*. Wiley.
- Hu, Y.-L., Farrell, R. M., Neufeld, C. J., Iza, M., Cruz, S. C., Pfaff, N., . . . others (2012). Effect of quantum well cap layer thickness on the microstructure and performance of InGaN/GaN solar cells. *Applied Physics Letters*, 100(16), 161101.
- Hurni, C. A., David, A., Cich, M. J., Aldaz, R. I., Ellis, B., Huang, K., . . . others (2015). Bulk GaN flip-chip violet light-emitting diodes with optimized efficiency for high-power operation. *Applied Physics Letters*, 106(3), 031101.
- Imer, B., Speck, J., DenBaars, S., & Nakamura, S. (2012). *Growth of non-polar m-plane III-nitride film using metalorganic chemical vapor deposition (MOCVD)*. Retrieved on 2 January 2018, <https://www.google.com/patents/US8097481>. (US Patent 8,097,481)

- Jan, Y.-K., & Lin, C.-A. (1998). Lamp configuration design for rapid thermal processing systems. *IEEE transactions on Semiconductor Manufacturing*, 11(1), 75–84.
- Jin, Z., Fang, H., Yang, N., Zhang, Z., Wang, S., & Xu, J. (2014). Influence of temperature-dependent thermophysical properties of sapphire on the modeling of kyropoulos cooling process. *Journal of Crystal Growth*, 405, 52–58.
- Kim, K.-C., Schmidt, M. C., Sato, H., Wu, F., Fellows, N., Saito, M., . . . DenBaars, S. P. (2007). Improved electroluminescence on nonpolar m-plane InGaN/GaN quantum wells LEDs. *physica status solidi (RRL)-Rapid Research Letters*, 1(3), 125–127.
- Krames, M. (2013). Light-emitting diodes: GaN-on-GaN platform removes cost/performance tradeoffs in led lighting. *Laser Focus World*, 49(9), 37.
- Krost, A., & Dadgar, A. (2002). GaN-based optoelectronics on silicon substrates. *Materials Science and Engineering: B*, 93(1-3), 77–84.
- Kumar. (2013). *Uv-vis and photoluminescence spectroscopy for nanomaterials characterization*. Springer Berlin Heidelberg.
- Kumar, Park, J., Lee, Y., Chung, S., Hong, C., & Suh, E. (2007). Effect of barrier growth temperature on morphological evolution of green InGaN/GaN multi-quantum well heterostructures. *Journal of Physics D: Applied Physics*, 40(17), 5050.
- Lai, K., Paskova, T., Wheeler, V., Chung, T., Grenko, J., Johnson, M., . . . Evans, K. (2012). Indium incorporation in InGaN/GaN quantum wells grown on m-plane GaN substrate and c-plane sapphire. *Physica Status Solidi*, 209(3), 559–564.
- Lai, K., Paskova, T., Wheeler, V., Grenko, J., Johnson, M., Barlage, D., . . . Evans, K. (2009). Excitation current dependent cathodoluminescence study of InGaN/GaN quantum wells grown on m-plane and c-plane GaN substrates. *Journal of Applied Physics*, 106(11), 113104.
- Lee, S., Kwon, S. Y., & Ham, H. J. (2011). Specific heat capacity of gallium nitride. *Japanese Journal of Applied Physics*, 50(11S), 11RG02.
- Leem, S. J., Shin, Y. C., Kim, K. C., Kim, E. H., Sung, Y. M., Moon, Y., . . . Kim, T. G. (2008). The effect of the low-mole InGaN structure and InGaN/GaN strained layer superlattices on optical performance of multiple quantum well active layers. *Journal of Crystal Growth*, 311(1), 103–106.
- Lojek, B. (2007). *History of semiconductor engineering*. Springer.

- Markov, I. (1995). *Crystal growth for beginners: Fundamentals of nucleation, crystal growth and epitaxy*. World Scientific.
- Maruska, H. á., & Tietjen, J. (1969). The preparation and properties of vapor-deposited single-crystal-line GaN. *Applied Physics Letters*, 15(10), 327–329.
- Matheson. (2015). *Metal organic chemical vapor deposition mocvd*. Retrieved on 12 April 2018, <https://www.mathesongas.com>.
- Miguel, J., et al. (2014). Computational calculation of the electronic and magnetic properties of 1x1-mn/GaN (M= V, Cr and Mn) multilayers. *International Journal of Physical Sciences*, 9(24), 538–544.
- Mo, Y.-W., Savage, D., Swartzentruber, B., & Lagally, M. G. (1990). Kinetic pathway in stranski-krastanov growth of Ge on Si (001). *Physical Review Letters*, 65(8), 1020.
- Moram, M., Ghedia, C., Rao, D., Barnard, J., Zhang, Y., Kappers, M., & Humphreys, C. (2009). On the origin of threading dislocations in GaN films. *Journal of Applied Physics*, 106(7), 073513.
- Moram, M., & Vickers, M. (2009). X-ray diffraction of III-nitrides. *Reports on Progress in Physics*, 72(3), 036502.
- Nakamura, S., Iwasa, N., Senoh, M., & Mukai, T. (1992). Hole compensation mechanism of p-type GaN films. *Japanese Journal of Applied Physics*, 31(5R), 1258.
- Nakamura, S., & Krames, M. R. (2013). History of gallium–nitride-based light-emitting diodes for illumination. *Proceedings of the IEEE*, 101(10), 2211–2220.
- Nakamura, S., Pearton, S., & Fasol, G. (2013). *The blue laser diode: the complete story*. Springer Science & Business Media.
- Narukawa, Y., Ichikawa, M., Sanga, D., Sano, M., & Mukai, T. (2010). White light emitting diodes with super-high luminous efficacy. *Journal of Physics D: Applied Physics*, 43(35), 354002.
- Neumark, G., Kuskovsky, I., & Jiang, H. (2007). *Wide bandgap light emitting materials and devices*. Wiley.
- Öztürk, M., Hongbo, Y., Sarıkavak, B., Korcak, S., Özçelik, S., & Özbay, E. (2010). Structural analysis of an InGaN/GaN based light emitting diode by x-ray diffraction. *Journal of Materials Science: Materials in Electronics*, 21(2), 185–191.

- Paskova, T., Hanser, D. A., & Evans, K. R. (2010). GaN substrates for III-nitride devices. *Proceedings of the IEEE*, 98(7), 1324–1338.
- Popovic, R. (2003). *Hall effect devices, second edition*. CRC Press.
- Pryor, R. W. (2009). *Multiphysics modeling using comsol: a first principles approach*. Jones & Bartlett Publishers.
- Quan, Z., Liu, J., Fang, F., Wang, G., & Jiang, F. (2015). A new interpretation for performance improvement of high-efficiency vertical blue light-emitting diodes by ingan/gan superlattices. *Journal of Applied Physics*, 118(19), 193102.
- Rais-Zadeh, M., Gokhale, V. J., Ansari, A., Faucher, M., Théron, D., Cordier, Y., & Buchailot, L. (2014). Gallium nitride as an electromechanical material. *Journal of Microelectromechanical Systems*, 23(6), 1252–1271.
- Ren, C. (2016). Polarisation fields in III-nitrides: effects and control. *Materials Science and Technology*, 32(5), 418–433.
- Roozeboom, F. (2013). *Advances in rapid thermal and integrated processing*. Springer Netherlands.
- Seong, T., Han, J., Amano, H., & Morkoc, H. (2014). *III-nitride based light emitting diodes and applications*. Springer Netherlands.
- Shang, L., Lu, T., Zhai, G., Jia, Z., Zhang, H., Ma, S., . . . Xu, B. (2015). The evolution of a GaN/sapphire interface with different nucleation layer thickness during two-step growth and its influence on the bulk GaN crystal quality. *RSC Advances*, 5(63), 51201–51207.
- Sheen, M.-H., Kim, S.-D., Lee, J.-H., Shim, J.-I., & Kim, Y.-W. (2015). V-pits as barriers to diffusion of carriers in ingan/gan quantum wells. *Journal of Electronic Materials*, 44(11), 4134–4138.
- Shibata, H., Waseda, Y., Ohta, H., Kiyomi, K., Shimoyama, K., Fujito, K., . . . Fukuda, T. (2007). High thermal conductivity of gallium nitride (GaN) crystals grown by HVPE process. *Materials Transactions*, 48(10), 2782–2786.
- Speck, J., & Chichibu, S. (2009). Nonpolar and semipolar group III nitride-based materials. *MRS Bulletin*, 34(5), 304–312.
- Stringfellow, G. (2012). *Organometallic vapor-phase epitaxy: Theory and practice*. Elsevier Science.

- Tyagi, A., Zhong, H., Fellows, N. N., Iza, M., Speck, J. S., DenBaars, S. P., & Nakamura, S. (2007). High brightness violet InGaN/GaN light emitting diodes on semipolar (1011) bulk GaN substrates. *Japanese Journal of Applied Physics*, 46(2L), L129.
- Van der Heide, P. (2014). *Secondary ion mass spectrometry: An introduction to principles and practices*. Wiley.
- Vickers, M., Kappers, M., Smeeton, T., Thrush, E., Barnard, J., & Humphreys, C. (2003). Determination of the indium content and layer thicknesses in InGaN/GaN quantum wells by x-ray scattering. *Journal of Applied Physics*, 94(3), 1565–1574.
- Young, N., Farrell, R., Hu, Y., Terao, Y., Iza, M., Keller, S., . . . Speck, J. (2013). High performance thin quantum barrier InGaN/GaN solar cells on sapphire and bulk (0001) GaN substrates. *Applied Physics Letters*, 103(17), 173903.
- Zhao, Y., Tanaka, S., Pan, C.-C., Fujito, K., Feezell, D., Speck, J. S., . . . Nakamura, S. (2011). High-power blue-violet semipolar (2011) InGaN/GaN light-emitting diodes with low efficiency droop at 200 A/cm². *Applied Physics Express*, 4(8), 082104.

LIST OF PUBLICATIONS AND PAPERS PRESENTED

Sivanathan, P.C., Shuhaimi, A., Hamza, H., Kowsz, S. J., Khudus, M. I. A., Li, H., & Allif, K. (2018). Effect of thermal interaction between bulk GaN substrates and corral sapphire on blue light emission InGaN/GaN multi-quantum wells by MOCVD. *Superlattices and Microstructures*, 119, 157–165.

University of Malaya